Acoustic emission waveform analysis in CFRP under Mode I test

ACOUSTIC EMISSION WAVEFORMS FOR DAMAGE MONITORING IN COMPOSITE MATERIALS: SHIFTING IN SPECTRAL DENSITY, ENTROPY AND WAVELET PACKET TRANSFORM

Claudia Barile [a], Caterina Casavola [a], Giovanni Pappalettera [a], Vimalathithan Paramsamy Kannan [a]

[a] Dipartimento di Meccanica, Matematica e Management, Politecnico di Bari, Via Orabana 4, 70125 – Bari, Italy

Abstract

Signal-based acoustic emission data is analysed in this research work for identifying the damage modes in Carbon Fiber Reinforced Plastic (CFRP) composites. The research work is divided into three parts: analysis of the shifting in the spectral density of acoustic waveforms, use of Waveform Entropy for selecting the best wavelet and implementation of Wavelet Packet Transform (WPT) for identifying the damage process. The first two methodologies introduced in this research work are novel. Shifting in the spectral density is introduced in analogous to 'flicker noise' which is popular in the field of waveform processing. The entropy based wavelet selection is refined by using quadratic Renyi's entropy and comparing the spectral energy of the dominating frequency band of the acoustic waveforms. The methodologies introduced in this research work are promising. They serve the purpose of identifying the damage process effectively in the CFRP composites.

Keywords: Acoustic emission; Mode I delamination; Flicker noise; Wavelet entropy; Wavelet Packet Transform

1. Introduction

Since the beginning of the 21st century, the usage of Acoustic Emission (AE) testing for structures has increased exponentially [1]. This incredible growth can be attributed to the development of more liberal tools and methodologies for monitoring and processing acoustic data. Consequently, a variety of new methodologies have been introduced for extracting information from the recorded acoustic data. One of the areas which has used AE techniques more commonly over the last few years is the damage process monitoring in composite structures [2].

The processing of the acoustic data can be generalized into two categories, albeit not strictly: parameter-based data processing and signal-based data processing. The parameter-based data processing involves extracting the descriptors which can define the characteristics of each recorded AE event and analysing them. The descriptors include peak amplitude in decibels, acoustic energy, number of counts crossing the detection threshold in an acoustic event, duration of the AE signal, absolute energy in aJ, signal strength, rise angle, decay angle, etc [3, 4].

The signal-based data processing involves analysing the recorded AE signals in their frequency domain or time-frequency domain. This also includes the denoising of the AE signals and the decomposition of the signals to extract the required information. Various wavelet and waveform analysis techniques have been explored over the years in the field of AE for assessing the damage process in composite structures. Some of the most abundantly used techniques include Fast Fourier Transform (FFT), Continuous Wavelet Transform (CWT), Discrete Wavelet Transform (DWT) and Wavelet Packet Transform (WPT) [5 – 7]. Apart from this waveform and wavelet transforms, some other Adaptive Wavelet Transform (AWT) or Hilbert-Huang Transform (HHT) has also been used by some researchers. The FFT and HHT provide information about the AE signal in its frequency domain, while CWT and DWT provide a detailed time-frequency analysis.

Both the parameter-based and signal-based analysis of an AE signal have their advantages and limitations. The debate on which is more suited for analysing an AE signal for damage process monitoring in composite structures is still open and can lead to different answers in the context of the problem.

In this research work, the signal-based analysis is considered for processing the acoustic data to monitor the damage process in composite materials. The research work comprises of three parts: a) analysis of the shifting in the spectral density of AE signal during damage process b) Selection of the best wavelet for Wavelet Transform (WT) using entropy c) implementation of WPT using the selected wavelet for damage process identification.

The novelty of this research work lies in the usage of these methodologies innovatively and efficiently for the damage process monitoring of composite materials. The material used for this study is Carbon Fiber Reinforced Plastic (CFRP) composite in

Mode I delamination configuration. The acoustic data recorded during the Mode I delamination test has been used for validating the aforementioned methodologies.

Section 2 of this paper presents the introduction and detailed explanations of the methodologies used in this research work. Section 3 details the information about the material used and the test procedure followed for Mode I delamination and the acquisition of AE data during the testing. Section 4 explains the selection of the acoustic waveforms from the large dataset for processing. Section 5 is dedicated to explaining the results obtained and also the summary of the results obtained using the three methodologies. An attempt has been made to string together the results obtained from the three methodologies.

2. Proposed Methodology for Processing Acoustic Emission data

2.1 Shifting of the Acoustic Signal

MacDonald quoted in 1962 that many researchers considered fluctuations or noise as rather esoteric or perhaps even pointless. Besides, spontaneous fluctuations were considered as an unnecessary evil [8, 9]. Although these quotes are referred to the fluctuations or electrical noise in solids (for instance, a simple resistor), they can be stretched also to the acoustic signals. These shiftings in the acoustic signal are ignored consistently by most of the researchers. For instance, the most traditional and frequently used method of analysing an acoustic waveform in its frequency domain is the FFT analysis. It provides the spectral density of the recorded waveform in different frequency domains. Most researchers normally consider only the frequency with the largest spectral density (peak frequency) for analysis and ignore the fluctuations or shifting in the spectral density [10]. While some researchers have used other frequency components such as Frequency Centroid or Weighted Peak Frequency, the significance of the shifting is rather ignored [4, 11].

The characteristics of the flicker noise observed across the voltage drop in a resistor can be explained by the phenomenological equation by Hooge [12]:

$$S(f) = \gamma \frac{V_{DC}^{2+\beta}}{N_c f^{\alpha}} \tag{1}$$

where, $S(f)$ is the spectral density, V_{DC} is the average voltage drop across the solid resistor, N_c is the number of charge carriers in the solid, f is the frequency, α, β and γ are constants ($\beta \approx 0$).

Equation (1) has been simplified for the general understanding of the shifting as follows [11]:

$$S(f) = \gamma f^{-\alpha} \tag{2}$$

Applying logarithm on both sides of Equation (2) yields,

$$\log[S(f)] = \log\gamma - \alpha \log(f) \tag{3}$$

The signal characteristics and its shifting can be categorized based on the slope coefficient α. In the various fields of science, based on the values of the scalar coefficient α, the signal characteristics can be categorized into white noise, pink noise and brown noise [13]. The white noise, which has constant spectral energy is observed when $\alpha = 0$. The terms pink noise and brown noise are used to identify the fluctuations when α is 1 and 2, respectively.

The shifting of the spectral density and the characteristics of the signals based on the different types of noises (according to Equation (3)) have been used in many fields including geological, bioengineering, pedagogical, physiological and musical phenomena. Nonetheless, the fluctuations used in these fields are based on the low-frequency signals [13, 14, 15]. The term '1/f noise' or flicker noise is commonly used to refer to these fluctuations or the shifting, which is common in the field of signal processing.

Although the term flicker noise is referred to the low-frequency fluctuations, this phenomenon can be extended to medium to high frequency signals. This has been explained theoretically by Dutta and Horn. Recently, Carpinteri et. al. [16] and Freidrich et. al. [17] have used the flicker noise for damage process monitoring in concrete structures and Glass Fiber Reinforced Polymers (GFRP), respectively. Carpinteri et. al. [16] studied the flicker noise of the acoustic signals released from the concrete structures for identifying the critical conditions of the structure. The AE signals generated during a damage process in quasi-brittle materials such as concrete vary largely from the unstable transient signals generated in Fiber Reinforced Polymer (FRP) composites. Freidrich et. al. [17] have studied the flicker noise or fluctuations of acoustic signals ranging from 5 Hz to 60 kHz in GFRP. The acoustic signals emitted from a damage process in a composite

material normally range from a few kHz to MHz. Acoustic signals released from different damage modes in CFRP normally have peak frequency ranges from 150 kHz to 500 kHz. For instance, the fiber breakage event in a CFRP can release acoustic signals with a peak frequency of 450 kHz to 500 kHz. So, in this research work, the concept of flicker noise is extended to the shifting in the signal. Instead of analysing the noise in the low frequency content, the shifting in the signal is analysed. In this study, the term shifting is introduced in the sense that different slopes with which the spectral density fluctuates are used. The details are explained in detail in Section 5.3.

Since the shifting of the spectral density is studied for high frequency signals, without strictly bound by the values of α in Equation (2) to represent the different noise types, the term 'flicker noise' or '1/f noise' has not been used from this instance. Rather, the term "shifting of the spectral density" will be used throughout this article.

2.2 Selecting the best Wavelet using Entropy

The entropy of the waveform is used as the main identifier for selecting the suitable wavelet for analysis. Thus, this section is started with a brief introduction about it and is followed by the procedure for using it. In the field of physics and mathematics, entropy is defined as the measure of information contained in a waveform [18 – 20]. Theoretically, entropy is the measure of randomness or the instability contained in a probability distribution. Many entropy definitions exist in different fields and they are not suitable for all applications. A review of the different definitions of entropy and the generalized form of entropy is provided by Amigó et. al. [21] With respect to this research work, the entropy of a waveform can be defined as the measure of information in it [22].

For a waveform having a random distribution of amplitude as $\{s_1, s_2, s_3, \dots, s_n\}$, the generalized form of entropy $H_a(s)$ can be given as [23],

$$H_a(s) = \frac{1}{1-a}\log\left(\sum_{k=1}^{n}[P(s_k)]^a\right) \tag{4}$$

where, $P(s_k)$ is the discrete probability distribution of the amplitude.

The generalized form of entropy defined in Equation (4) can be described as Renyi's entropy [23, 24]. The choice in the selection of the constant a in Renyi's entropy is its most interesting property. However, the choice in the selection of a is bound to some

constraints based on the probability of the distribution of data. Considering the waveform as an example, when $a > 1$, more weightage is given to the amplitude with high probability. Conversely, when $a < 1$, more weightage is given to the amplitude in the distribution with low probability [25, 26]. Based on the value of a, Renyi's entropy can take different forms.

When the value of a approaches close to '0', Equation 4 is transformed to give Maximum entropy or Hartley's entropy [27].

$$H_0(s) = \log n \tag{5}$$

When the value of a reaches 1, the limiting value of the entropy can be defined as Shannon's entropy, which is provided in Equation (6). In fact, Shannon extended Hartley's theory of entropy in Equation (5) by introducing the weightage function to present Shannon's entropy [28]. Shannon's entropy is by far the most used form of entropy in many fields, including information theory and cryptography [29, 30].

$$H_1(s) = \sum_{k=1}^{n} P(s_k) \log[P(s_k)] \tag{6}$$

The quadratic Renyi's entropy, which is used in this research work is derived when the value of a reaches 2 [23, 24]. The quadratic Renyi's entropy presented in Equation (7) is used in this research work.

$$H(s) = -\log\left(\sum_{k=1}^{n} [P(s_k)]^2\right) \tag{7}$$

Many researchers have generalized the applications of Renyi's entropy and its advantages over using Shannon's entropy in different fields [21, 24, 31, 32]. The consensus is that Renyi's entropy is more applicable for a random search and statistical waveform processing. Based on these observations, Renyi's entropy is selected for this study.

Several researchers have used Shannon's entropy in processing acoustic waveforms but Renyi's entropy is seldom used. Tanvir et. al. has used Renyi's entropy of the acoustic waveform in defining the characteristics of the fatigue damage evolution [24]. But the application in which they used Renyi's entropy is debatable. Tanvir et. al. used cumulative Renyi's entropy, which is necessarily the sum of the measures of randomness, as an acoustic descriptor for damage evolution [24].

In this research work, however, Renyi's entropy is used for the selection of optimum wavelet for processing the acoustic waveforms. Selecting a wavelet for the WT processing is very essential. The maximum information of the waveforms in their time-frequency domain and the distribution of spectral energy in the different frequency bands is based on the selection of the best wavelet. In the field of damage process monitoring using acoustic waveforms, no definite procedures for selecting the best wavelet have been studied extensively. In other similar fields, where acoustic waveforms are used, the Energy-to-Shannon Entropy ratio is used [31, 32].

On one hand, since waveform entropy is the measure of the randomness or instability in a waveform, it is safe to assume that the lower value of entropy defines the stability in an acoustic waveform. On the other hand, measuring the energy coefficients of an acoustic waveform using some WT methods should yield the largest energy possible. Combining these two necessities, a ratio called η has been established.

$$\eta = \frac{E_{WT}}{H(s)} \tag{8}$$

E_{WT} is the energy coefficient of the waveform measured using WT.

Basically, the η value is based on selecting the waveforms which yields high energy coefficient with low instabilities. The procedure for calculating the quadratic Renyi's entropy, E_{WT}, η value and the selection of the best wavelet is explained below.

Discrete Wavelet Transform (DWT) is used for the calculation of both $H(s)$ and E_{WT}. The DWT decomposition of the acoustic waveforms is performed in the programming module of MATLAB® [33, 34]. MATLAB® provides the possibility of selecting different wavelets for the DWT.

Let us consider an acoustic waveform $f(t)$, which can be expressed as,

$$f(t) = \{s_1, s_2, s_3, \dots, s_n\}^T \tag{9}$$

where, n is the length of the waveform. If the waveform $f(t)$ is decomposed using a wavelet $\Psi(t)$, the DWT of the waveform can be given as,

$$WT_j = \langle f(t), \Psi_j(t) \rangle \tag{10}$$

where, j is the number of the selected wavelet. The DWT results will be in the form,

$$WT_j = \{wt_1, wt_2, wt_3, \dots, wt_n\}^T \tag{11}$$

The energy coefficient E_{WT} is calculated as,

$$E_{WT} = \sum_{k=1}^{n} \left| wt_{j,k} \right|^2 \tag{12}$$

The discrete probability in Equation (7) for calculating the quadratic Renyi's entropy is calculated as follows [29]:

$$p(x_k) = \frac{|wt_k|^2}{\sum_{i=1}^{n} \left| WT_{j,i} \right|^2} \tag{13}$$

Now by using $p(x_i)$, from Equation (7), the quadratic Renyi's entropy $H(x)$ can be calculated. From E_{WT} calculated using Equation (12) and $H(x)$ calculated using Equation (7), the η value can be calculated using Equation (8).

The same procedure is repeated for different mother wavelets $\Psi(t)$. In this research work, 24 wavelets are used for comparison. Theoretically, the wavelet which produces the highest value of η is selected as the best wavelet for further analysis.

However, the η value cannot be considered carelessly because it represents the entropy and energy coefficient measured from a very transient and instable acoustic waveform. The possibility of η value to be very close between different wavelets cannot be ignored either. For this reason, another new approach has been introduced in this research work.

Which wavelet can recover the maximum spectral energy from an acoustic waveform after processing, especially in the dominating frequency band? Answering this question is possibly the best way to choose the optimal wavelet by overcoming the suspicions of using the η value.

In this research work, η value is primarily used for selecting the 3 most suitable wavelets. Following that, the recovery of maximum spectral energy in the dominating frequency band of the acoustic signal is used for selecting the best wavelet among the previously selected 3. For recovering the spectral energies of the waveform in different frequency domains, Wavelet Packet Transform (WPT) is used [6, 35, 36]. The procedure followed for selecting the best wavelet using the WPT is explained below.

WPT using the selected 3 wavelets are used for decomposing the acoustic signal into 3 different levels N. Decomposing using WPT in 3 levels will give the spectral energy of $2^N = 8$ components C. For example,

$$WPT_j = \langle f(t), \Psi_j(t) \rangle \tag{14}$$

WPT_j for the wavelet $\Psi_j(t)$ will be in the form,

$$WPT_j = \left| W_{j,1}, W_{j,2}, W_{j,3}, \dots, W_{j,8} \right| \tag{15}$$

where, $W_{j,C}$ is the spectral energy of the waveform distributed in the component C. If the same process is repeated for the 3 wavelets selected using η value, a comparison between the spectral energy recovered in different components using the 3 different wavelets can be made. The wavelet which has recovered the maximum spectral energy in the dominating frequency band, $\max W_{j,C} \{for\ C = 1,2,3, \dots 8\}$ can be selected as the best wavelet for further analysis.

2.3 Wavelet Packet Transform for damage process monitoring

In our previous research works, the wavelet packet transform has been used successfully in identifying the damage process [6]. Nonetheless, the wavelet used in that research work was 'sym8'. No selection procedure was followed in that research work. In this present research work, the best wavelet is selected from a list of 24 wavelets using the procedures explained in Section 2.2 and the selected wavelet is used for decomposing the acoustic waveforms into 8 components. Each of these components comprises the spectral energy of the waveform distributed in the time domain of a specific frequency band. By analysing the spectral energy of the waveforms in their time-frequency domain, the damage process can be monitored.

Typically, in a CFRP material, which is used in this research work, the macroscopic damage modes can be generalized into matrix cracking, delamination, debonding between the matrix and the fibers, fiber breakage, fiber pullout and through-thickness (interlaminar) crack growth [3, 4, 37, 38]. Over the years, several researchers experimentally validated the frequency band of the acoustic signal associated with the different damage processes. For example, an acoustic event generated as a consequence of matrix cracking or delamination will have the characteristic frequency range of 150 kHz to 200 kHz. At the same time, the acoustic event generated due to fiber breakage will be above 300 kHz or 350 kHz [37 – 42]. Although most of these results are provided

through the FFT analysis and the peak amplitude values, several researchers have used CWT and WPT for proving the same. The reason for choosing CWT or WPT over the conventional FFT is because they can provide information on the acoustic waveforms in their time domain. Events such as matrix cracking or delamination release acoustic signals with longer duration [6]. On the other hand, the fiber breakage or crack growth releases very transient signals with shorter duration and high frequency. Thus, it is essential to understand the characteristics of the signals also in their time domain.

These observations, indeed, are not without debates. Some researchers have argued that the acoustic events with frequency above 350 kHz does not necessarily represent fiber breakage at all the time and it could also represent the acoustic events released from the interlaminar crack growth [11, 42]. The experimental evidence has also been provided for the same. This is the reason why the WPT becomes more essential in the damage process monitoring. Because the WPT provides the characteristics of the different frequency bands associated with the recorded acoustic waveforms in their time-frequency domain. So, overall characteristics of the acoustic signal can be obtained. Using this, the damage process associated with the composite material, to an extent also with the structure can be analysed. As indicated in Section 1, the damage process characteristics in CFRP specimen subjected to mode I delamination is studied in this research work.

3. Experimental Procedure

The material used for testing in this research work is CFRP prepared using the Resin Film Infusion (RFI) process. The CFRP system has 35% resin content with high strength carbon fibers reinforced unidirectionally in the matrix. The unidirectional specimens are prepared by inserting a non-adhesive insert of thickness 13 μm (approx.) and a length of 45 mm to create the precrack [43]. The specimen has an even number of plies with each unidirectional ply having a thickness of 0.152 mm. The CFRP slab is cut into DCB configuration according to ASTM D5528 - Standard Test Method for Mode I Interlaminar Fracture Toughness of Unidirectional Fiber-Reinforced Polymer Matrix Composites [44]. The length, breadth and thickness of each specimen are 125 mm, 25 mm and 3 mm, respectively. A pair of piano hinges are attached to the mouth of the specimen where the adhesive insert is placed. The piano hinges are attached through a strong epoxy adhesive. The configuration of the specimen is presented in Figure 1.

The Double Cantilever Beam (DCB) is carried out on INSTRON servo-hydraulic testing machine at a constant displacement rate of 1 mm/min. A total of 3 specimens named A, B and C are tested for this study.

Figure 1. Configuration of DCB specimen

For recording the acoustic signals released during the damage process, a piezoelectric sensor was attached to the surface of the specimen. Silica gel is used as a coupling agent between the surface of the specimen and the sensor to provide good acoustic coupling and to avoid recording the reverberating signals. The sensor used in this study is R30α – general purpose sensor with an operating frequency of 150 kHz to 400 kHz and a peak sensitivity of 54 dB. The threshold for the acquisition of the AE signals is set as 35 dB. The recorded acoustic signals are pre-amplified by 40 dB using 2/4/6 AE preamplifier. The signals are further filtered through low-pass and high-pass filters between 1 kHz and 3MHz, respectively. The signals are processed at PAC PCI 2 data acquisition system. The length of the waveform recorded is set as 1K and the waveforms are recorded at a sampling rate of 1 mega sample per second (1 MSps).

4. Selection of Acoustic Emission data

During the DCB tests in all three specimens, a large number of acoustic hits are recorded. The total number of acoustic hits recorded and the duration of the DCB test for all three specimens are presented in Table 1. Besides, the distribution of the number of acoustic hits throughout the test is presented in Figure 2.

Table 1. Duration of the DCB test and the total number of Acoustic Hits recorded for all specimens

From Table 1, it can be observed that approximately 20000 AE hits are recorded during each test. For selecting the best wavelet using entropy, $H(x)$, E_{WT} and R values for all the acoustic hits are calculated and their mean values are taken for comparison. However, for WPT, analysing 20000 acoustic waveforms has some perennial problems. First, analysing all the waveforms is time-consuming and it also consumes a large amount of storage space. (For the sake of simplicity, the number of acoustic waveforms recorded in all the specimens will be indicated as 20000 from herein)

As shown in Figure 2, the distribution of the acoustic hits is not uniform throughout the test. Considering this, a set of representative waveforms can be selected from the distributed waveforms for further analysis. Again, there is no definite set of rules of selecting the waveforms from a representative group. For this reason, the waveforms are selected based on the load response of the DCB specimens under the delamination.

Figure 3 shows the load responses of the specimens plotted over the duration of the test along with the cumulative number of hits. Specimens A and B have 3 load peaks while specimen C has only one load peak, which occurs before the specimen starts losing its load bearing property. Based on the load peaks, the cumulative number of hits, the load regions are separated into 3. For each specimen, 3 waveforms from each region, so a total of 9 specimens are taken for this study. The details about the load responses, the reasons for the multiple peaks and other details about the mechanical performances of the three specimens can be found in our previous research work.

Figure 2. Distribution of the acoustic hits recorded during the entire duration of the test for specimens (a) A, (b) B and (c) C

Figure 3. Load responses of the DCB specimens plotted over the duration of the test along with the cumulative hits for specimens (a) A, (b) B and (c) C

5. Results and Discussions

5.1 Selection of Wavelet using Entropy

In this research work, 5 different wavelet families and a total of 24 wavelets are compared and the best wavelet is selected for the WPT analysis. The wavelet families and the list of wavelets used in this study are presented in Table 2. The wavelet families and wavelets are selected based on the literature survey made on the application of these wavelets in acoustic emission waveforms and similar transient signals.

Table 2. Wavelet Families and Wavelet selected for the analysis

The quadratic Renyi's entropy $H(s)$, the energy coefficient of the wavelet E_{WT} and the η values calculated using Equations (7), (12) and (8) for all the acoustic waveforms as presented in Table 3 for all the 3 specimens. The average value of $H(s)$, E_{WT} and η

value are calculated for the 24 wavelets. They are ranked based on the largest value of η and are presented in Table 3.

Table 3. Average quadratic Renyi's Entropy, Average Wavelet Energy, η Value and Rank based on η Value for specimens A, B and C

From Table 3, it is very clear that the wavelets dmey, coif5 and coif4 secures the maximum values of η for all 3 specimens and consequently secures the best ranks. While looking at the η values in the Rank 1, 2 and 3 and also between Rank 3 and Rank 4 wavelets, there is not a great difference between them. This is the reason why the η value is not taken very casually and considered 'dmey' as the best wavelet without further scrutinizing.

Using WPT with the wavelets dmey, coif5 and coif4, the acoustic waveforms are decomposed into 8 components. The spectral energy of the waveforms recorded in specimens A, B and C in each of the components are presented in Table 4, Table 5 and Table 6, respectively.

Naturally, the spectral energy of the 20000 waveforms must be decomposed and analysed for comparison. But presenting 20000 waveforms results is redundant and thus the selected 9 acoustic waveforms from each specimen, as indicated in Section 4 are presented in Table 4, Table 5 and Table 6.

Table 4. WPT components for the selected waveforms from Specimen A calculated using selected wavelets coif4, coif5 and dmey

Table 5. WPT components for the selected waveforms from Specimen B calculated using selected wavelets coif4, coif5 and dmey

Table 6. WPT components for the selected waveforms from Specimen C calculated using selected wavelets coif4, coif5 and dmey

The dominating frequency of each waveform differs from one another. Because each of these dominating frequency bands represents the different types of damage modes from which the acoustic signals are released. The discussion about the different damage modes will be presented in the next section.

In Table 4, the results of specimen A are presented. It can be clearly seen that the dominating frequency is either in the frequency band 125 kHz to 187.5 kHz or 187.5 kHz to 250 kHz. The wavelet 'dmey' has recovered most of the spectral energy in all the selected waveforms. However, in Table 5, the results of specimen B shows that in some waveforms, the 'coif5' has recovered most of the spectral energy, albeit it is not observed among all the selected 9 waveforms. Table 6 shows the spectral energy of the waveforms from specimen C. Specimen C shows similar results to Specimen A; the wavelet 'dmey' has recovered most of the spectral energy. While also comparing the spectral energy of 20000 waveforms, a significantly large number of waveforms that have recovered the most spectral energy is when they are decomposed using 'dmey' wavelet. Therefore, 'dmey' wavelet is selected as the best wavelet for processing the acoustic signals in this study.

It must be understood that the 'dmey' wavelet is selected for the acoustic waveforms generated during the mode I delamination of CFRP specimens. This cannot be nonchalantly selected for processing all the acoustic waveforms generated from CFRP specimens. The generation and propagation of acoustic waveforms are strictly based on the material properties and their configuration. This has been experimentally observed in our previous research works [6]. Besides, different wavelets have been used for different applications by various researchers. A word of indication to show the novelty in this research work that those research works only uses the Energy-to-Shannon entropy ratio and the dominating frequency using WPT has not been used.

5.2 Identification of Damage Process using WPT

'dmey' wavelet has been selected as the most optimal wavelet for processing the acoustic waveforms in this study. The 9 acoustic waveforms selected from each specimen are decomposed using WPT with the dmey wavelet and their results are discussed in this section. The results are presented in two ways: a) table showing the percentage of spectral energy distributed in each frequency band b) figure showing the distribution of the spectral energy distributed in each frequency band. The figures are provided in addition to the table with the spectral energy percentages is because the frequency distribution in the time domain can be explained only through the figures.

The results of the acoustic waveforms recorded from specimen A are presented in Table 7 and Figure 4.

Table 7. Spectral Energy Percentage of the Waveforms recorded from Specimen A

From Table 7, it can be observed that the waveforms taken from the Region 1 of the load response in Specimen A, about 50% of spectral energy is distributed in 125 kHz to 187.5 kHz frequency band and about 20% of spectral energy is distributed in 62.5 kHz to 125 kHz frequency band. Typically, the acoustic signals with the frequency range between 100 kHz and 150 kHz correspond to the matrix cracking or micro-cracking events. This has been evidently supported by many researchers [6, 10, 11, 45]. Besides, Region 1 lies within the first 30 seconds of the duration of the test, which has a maximum load of about 40 N (refer to Figure 3(a)). Since the delamination proceeds only after the occurrence of micro-cracking due to the stiffness of the DCB specimens in the mode I delamination test, it is safe to assume that these waveforms represent the signals generated from the matrix cracking or micro-cracking events.

Figure 4. Spectral Energy Distribution in each frequency band for the waveforms recorded from Specimen A

In Region 2 of Specimen A, more than 84% of the spectral energy is distributed in 125 kHz to 187.5 kHz frequency band in Waveforms 4 and 5. In Waveform 6, about 64% of the energy is distributed in 125 kHz to 187.5 kHz (Table 7). Comparing these results with Figure 4, it can be observed that Waveforms 4 and 5 are distributed for a longer duration, whereas Waveform 6 is shorter. Typically, the acoustic waveforms with lower energy, lower frequency and longer distribution in the time domain represent the delamination or fiber/matrix debonding. This has been observed in our previous studies as well when compared with the parameter-based acoustic data [6, 11, 45]. Waveforms 4 and 5 possibly could represent the debonding and Waveform 6 due to its similarity with Waveforms 1-3 could indicate the occurrence of matrix cracking. It is nothing out of ordinary to observe the occurrences of matrix cracking during any instances of the loading stage. Because the matrix cracking also leads to the friction of microparticles within the specimen, which can also release acoustic events. Most of these acoustic events also correspond to the frequency band of 100 kHz to 200 kHz.

In Region 3, in Waveforms 7 and 8, 25% of spectral energy distributed in 187.5 kHz to 250 kHz frequency band, while Waveform 8 has about 15%. These waveforms also have about 30% to 50% of the spectral energy distributed in the 125 kHz to 187.5 kHz frequency band. What is more interesting is that these waveforms also have a considerable amount of spectral energy distributed in higher frequency bands. Waveform 7 has about 15% in 375 kHz to 437.5 kHz and 14% in 437.5 kHz to 500 kHz. Waveform 8 and 9 have respectively 11% and 9% of spectral energy distributed in 437.5 kHz to 500 kHz frequency band. Comparing these results with Figure 4, the energy distributed are shorter in duration. Normally, acoustic signals with a frequency above 350 kHz or 400 kHz represents fiber breakage. Recently, Oz et. al has evidently shown that these higher frequencies can also represent the interlaminar crack growth [11]. Considering the geometrical configuration of the specimen, which is 0^{o} unidirectional and the nature of loading, mode I delamination, the chances for fiber breakage are very slim. Besides, no visible fiber breakages were observed in the ruptured specimens. Considering these possibilities, these waveforms can be attributed to the acoustic events due to the interlaminar crack (or through thickness) crack growth.

The spectral energy distribution of Specimen B is presented in Table 8 and Figure 5. The waveforms taken from Region 1 are not similar to the waveforms taken from the same region of Specimen A. In fact, Waveform 1 has about 29% of spectral energy distributed in the 437.5 kHz to 500 kHz frequency band, which is a phenomenon observed in Region 3 of Specimen A. This indicates that there is an interlaminar crack growth occurred in the early stages of loading in Specimen B. In fact, a small load peak at about 40 N is observed in Specimen B in Region 1 (Refer Figure 3(b)). This is followed by another load drop around the end of Region 1 at 60 N. These load drops could possibly be the indicators of the interlaminar crack growth occurring at the early stages of loading. In addition to that, Waveform 2 and 3 have spectral energy distributed in both 125 kHz to 187.5 kHz and 187.5 kHz to 250 kHz. Comparing with the distribution of these waveforms in the time domain from Figure 5, these possibly could represent the delamination. Apparently, specimen B has suffered both interlaminar crack growth and delamination at a very early stage. This could potentially be the reason for the two load drops in Region 1 before the end of 40 s of loading (Refer Figure 3(b)).

Table 8. Spectral Energy Percentage of the Waveforms recorded from Specimen B

The waveforms in Region 2 are also not comparable with the Region 2 of Specimen A. Waveform 4 has characteristics similar to that of acoustic events originating from matrix cracking with 71% of energy distributed in 125 kHz to 187.5 kHz and 25% in 62.5 kHz and 125 kHz frequency bands. Waveform 5 has the characteristics of interlaminar crack growth with 45% of the energy distributed in 125 kHz to 187.5 kHz and 27% of energy distributed in 437.5 kHz to 500 kHz frequency band. The same can be said also for Waveform 6 since it has the spectral energy distributed in 125 to 187.5 kHz, 187.5 kHz to 250 kHz and 375 kHz to 437.5 kHz frequency bands.

Waveform 7 from Region 3 is very much similar to the waveforms with the characteristics of the interlaminar crack growth. However, Waveforms 8 and 9 have about 60% of the spectral energy distributed in 62.5 kHz and 125 kHz frequency band and 30% of energy in 125 kHz to 187.5 kHz frequency band. These are the characteristics of acoustic events released from matrix cracking. It can be alluded similar to the previous occurrences of matrix cracking in any stage of the loading.

Figure 5. Spectral Energy Distribution in each frequency band for the waveforms recorded from Specimen B

The spectral energy results of Specimen C are presented in Table 9 and Figure 6. Waveforms 2 and 3 in Region 1 have about 80% of their spectral energy distributed in the frequency band 125 kHz to 187.5 kHz. This the indication of the acoustic events generated from matrix cracking, as it can also be compared with their shorter duration in Figure 6. Waveform 1 has a unique characteristic of 55% of the spectral energy distributed in 187.5 kHz to 250 kHz and 20% in 125 kHz to 187.5 kHz frequency band. Besides, the duration of Waveform 1 is very short so it cannot be correlated to the delamination [46]. At this moment, there are less significant evidence to correlate this waveform to any damage characteristics.

All the waveforms from Region 2 also have about 60% to 63% of their energy distributed in 125 kHz to 187.5 kHz and about 25% of the spectral energy in 187.5 kHz to 250 kHz. However, comparing these results with Figure 6, these waveforms are

distributed longer in the time domain. Thus, these waveforms may represent the acoustic signals generated from the delamination. The absence of interlaminar crack growth events in Specimen C in Regions 1 and 2 are in fact not surprising. If the load responses of Specimen A, B and C in Figure 3 are compared, it can be seen that Specimen 3 had carried load without any drop or bridging until it reaches the peak load of 115 N. The entire load response is very smooth indicating there are no other events than delamination occurred during the loading of Specimen C. Another argument can be placed to support this observation. The peak load of Specimen C is significantly larger than Specimen A and B and the specimen also carried load for a longer duration before final rupture (Refer Figure 3).

Table 9. Spectral Energy Percentage of the Waveforms recorded from Specimen C

Waveform 7 in Region 3 of Specimen C shows the characteristics of delamination with the spectral energies only distributed in 125 kHz to 187.5 kHz. Waveforms 8 and 9, however, has spectral energies distributed in 375 kHz to 437.5 kHz and 437.5 kHz to 500 kHz frequency bands. These waveforms represent interlaminar crack growth and they are taken from the final stages of the loading in Specimen C. This again proves the previous observation that Specimen C progressed through delamination smoothly until the final stage where the interlaminar crack growth occurs before the final rupture.

Figure 6. Spectral Energy Distribution in each frequency band for the waveforms recorded from Specimen C

From the above observations, it is safe to say that the WPT has the potential to identify the damage process in CFRP specimens since it can distinguish the acoustic signals based on the frequency and time domain characteristics. Nonetheless, it should be underlined that these waveforms are representatives of the loading stages. Extracting the dominating frequency band using WPT using the best wavelet can still distinguish the damage process in CFRP.

5.3 Shifting during damage process

Although the results of the WPT can identify the damage modes, there are some instances where the shifting is observed more frequently than the others. For instance, in

Figure 6, Waveforms 8 and 9 have two frequency bands sharing spectral energy at the same time duration. Thus, the occurrences of shifting must also be considered for an empirical study of waveforms. The aim of this section is not to identify the damage process using shifting. Rather, it is to use the damage process identified in the previous section for discussing shifting in the spectral density components of the frequency.

The shifting in the spectral density is calculated from the slopes between the logarithms of spectral density measured from FFT and the frequency. An example waveform for each specimen A, B and C, respectively, are presented in Figures 7, 8 and 9.

Figure 7. FFT results and Shifting in the spectral density of Waveform 1 from Specimen A

Figure 8. FFT results and Shifting in the spectral density of Waveform 1 from Specimen B

Figure 9. FFT results and Shifting in the spectral density of Waveform 1 from Specimen C

As shown in Figures 7, 8 and 9, the shifting in the spectral densities of the acoustic waveforms are characterized by three stages and each stage is represented by its slope and intercept. To avoid redundancy in displaying all the 27 waveforms analysed for this study, the slopes and intercept values of each stage in all the waveforms are presented in a tabular form. Table 10 summarizes the shifting in the waveforms taken from the testing of Specimen A and similarly Table 11 and Table 12, respectively are the results of Specimen B and C.

Table 10. Shifting in the Spectral Density of the Waveforms recorded from testing Specimen A

Before discussing the results of the shifting in the acoustic waveforms, it must be underlined that the delamination damage process could not be compared between the acoustic waveforms recorded in different specimens. Nonetheless, the shifting in the acoustic waveforms corresponding to the matrix cracking and interlaminar crack growth are comparable. The reason being that during the delamination process, the spectral energy is distributed between two close frequency bands, 125 kHz to 187.5 kHz and 187.5

kHz to 250 kHz. And the spectral energies sometimes are distributed more in the former and less in the latter frequency band and vice versa. This has been explained in Section 5.2. Because of this reason, the shifting of the spectral density also varies due to this variation in the energy distribution. Consequently, the acoustic waveforms generated from the delamination modes are not comparable in this section.

Table 11. Shifting in the Spectral Density of the Waveforms recorded from testing Specimen B

The acoustic waveforms that correspond to the interlaminar crack growth events from Specimen A are Waveforms 7, 8 and 9 (Table 10). Specimen B has Waveforms 1, 5, 6 and 7 corresponds to the interlaminar crack growth (Table 11). In the case of Specimen C, Waveforms 8 and 9 corresponds to the interlaminar crack growth event (Table 12). All these waveforms follow a very similar trend. The slope of the shift in Stage I is greater than -0.7 and it increases steeply with a positive slope in Stage II, which is followed by a negative slope that is above -3 in Stage III. The positive slope at Stage II of the crack growth events more or less lies around 3. There are few cases where there are outliers: Waveform 5 of Specimen B has a slope value of 6.0837 (Table 11) in Stage II and Waveform 8 of Specimen C with a slope value of 7.1647 (Table 12). Regardless of these outlying values, the trend in Stage I and Stage III are the same for all the waveforms recorded from the interlaminar crack growth events considered for this study.

Table 12. Shifting in the Spectral Density of the Waveforms recorded from testing Specimen C

Similarly, for the waveforms corresponding to the matrix cracking event, there is a strong relationship between the waveforms recorded in Specimen B and C. Waveforms 4, 8 and 9 of Specimen B (Table 11) and Waveforms 2 and 3 of Specimen C (Table 12) corresponds to the matrix cracking events. All these waveforms have the slope value between -0.75 and -0.7 in Stage I, which is followed by a steep increase with a positive slope in Stage II. In Stage III, the variation in the slope shifts steeply with a negative slope of less than -3. The important difference between the slope shifts in matrix cracking and crack growth event with respect to Stage III is that the negative slope is greater than -3 in waveforms corresponding to the interlaminar crack growth events, while it is less than -3 in the waveforms corresponding to the matrix cracking events.

Although the waveforms which correspond to the matrix cracking event in Specimen A (Waveforms 1, 2, 3 and 6 from Table 10) follows a similar trend in Stage I, II and III, the slope value in Stage I is not between -0.75 and -0.7, unlike the waveforms from Specimen B and C. Nonetheless, the trend of a steep increase in Stage II and a steep decrease in Stage III with the slope less than -3 is observed in these waveforms.

Although the delamination events cannot be strictly correlated to the slope values in either of the stages of shifting, the acoustic signals recorded from those events do not overlap the slope values representing the matrix cracking or crack growth. To summarize the slope values and trends of the shifts in the acoustic events, matrix cracking events normally have a negative slope between -0.75 and -0.7 in Stage I, followed by a steep increase with a positive slope in Stage II. In Stage III, it once again exhibits a negative slope of less than -3. The interlaminar crack growth events, on the other hand, have a negative slope of greater than -0.7 in Stage I, followed by a steep increase with a positive slope around 3 in Stage II. In Stage III, it exhibits a negative slope of greater than -3.

Since these shifting in the spectral density are introduced for the very first time in this research field, the results cannot be compared with any similar works. Although, the strong relationship between the shifting in the spectral density, particularly in the acoustic events corresponding to the matrix cracking and the interlaminar crack growth events can be observed. The necessity of an additional tool in processing acoustic waveforms is always necessary because these waveforms are very transient in nature and some waveform processing techniques are not suitable for analysing them under certain circumstances. For instance, in our previous research work, while studying the acoustic waveforms generated during a static testing of metallic specimens, CWT, DWT and WPT proved to be ineffective in studying these waveforms [47]. This is one of the main reasons why the shifting in the spectral density are explored in this research work, despite the damage modes are effectively identified using WPT.

Nevertheless, the shifting in the spectral density proves to be a promising methodology in processing the acoustic waveforms for assessing the damage process. It is essential to develop this further with a dedicated experimental campaign for analysing the acoustic signals generated from different damage processes in different materials.

6. Conclusion

In this research work, the signal-based acoustic data are processed for identifying the damage process in CFRP composites. Two new methodologies are introduced in this research work for this purpose. An entropy based method is introduced for selecting the most appropriate wavelet for processing the acoustic waveforms generated from the CFRP composites under mode I delamination. Using this technique, the 'dmey' wavelet is selected as the most appropriate wavelet for this study. Then this wavelet is used for decomposing the acoustic waveforms using Wavelet Packet Transform (WPT). The spectral energy distributed in different frequency bands from the WPT results is used to assess the damage process in the CFRP composites. The second methodology introduced in this research work is the shifting of spectral density. The shifting in the spectral density has been categorized into three stages with different slope values. By analysing the values of slopes in these three stages, the damage processes of matrix cracking and interlaminar crack growth have been identified.

Author Contributions

Conceptualization: Vimalathithan Paramsamy Kannan

Methodology: Vimalathithan Paramsamy Kannan, Claudia Barile, Giovanni Pappalettera

Validation: Vimalathithan Paramsamy Kannan, Claudia Barile, Giovanni Pappalettera

Formal analysis: Vimalathithan Paramsamy Kannan, Claudia Barile, Giovanni Pappalettera

Data Curation: Vimalathithan Paramsamy Kannan, Claudia Barile

Writing - Original Draft: Vimalathithan Paramsamy Kannan

Writing - Review & Editing: Vimalathithan Paramsamy Kannan, Claudia Barile, Giovanni Pappalettera

Supervision: Caterina Casavola

References

1. Hamstad, M.A., 2000. Thirty years of advances and some remaining challenges in the application of acoustic emission to composite materials. *Acoustic emission beyond the millennium*, pp.77-91.

2. Sause, M.G., 2016. *In situ monitoring of fiber-reinforced composites: theory, basic concepts, methods, and applications* (Vol. 242). Springer.

3. Saeedifar, M. and Zarouchas, D., 2020. Damage characterization of laminated composites using acoustic emission: A review. *Composites Part B: Engineering*, p.108039.

4. Barile, C., Casavola, C., Pappalettera, G. and Kannan, V.P., 2020. Application of different acoustic emission descriptors in damage assessment of fiber reinforced plastics: A comprehensive review. *Engineering Fracture Mechanics*, p.107083.

5. Sause, M.G., Müller, T., Horoschenkoff, A. and Horn, S., 2012. Quantification of failure mechanisms in mode-I loading of fiber reinforced plastics utilizing acoustic emission analysis. *Composites science and technology*, *72*(2), pp.167-174.

6. Barile, C., Casavola, C., Pappalettera, G. and Vimalathithan, P.K., 2019. Damage characterization in composite materials using acoustic emission signal-based and parameter-based data. *Composites Part B: Engineering*, *178*, p.107469.

7. Barile, C., Casavola, C., Pappalettera, G. and Vimalathithan, P.K., 2019. Experimental wavelet analysis of acoustic emission signal propagation in CFRP. *Engineering Fracture Mechanics*, *210*, pp.400-407.

8. MacDonald, D.K.C., 2006. *Noise and fluctuations: an introduction*. Courier Corporation.

9. Dutta, P. and Horn, P.M., 1981. Low-frequency fluctuations in solids: 1/f noise. *Reviews of Modern physics*, *53*(3), p.497.

10. Chandarana, N., Sanchez, D.M., Soutis, C. and Gresil, M., 2017. Early damage detection in composites during fabrication and mechanical testing. *Materials*, *10*(7), p.685.

11. Oz, F.E., Ersoy, N. and Lomov, S.V., 2017. Do high frequency acoustic emission events always represent fibre failure in CFRP laminates?. *Composites Part A: Applied Science and Manufacturing*, *103*, pp.230-235.

12. Hooge, F.N., 1969. 1/f noise is no surface effect. *Physics letters A*, *29*(3), pp.139-140.

13. Gilden, D.L., 2001. Cognitive emissions of 1/f noise. *Psychological review*, *108*(1), p.33.

14. Milotti, E., 2002. 1/f noise: a pedagogical review. *arXiv preprint physics/0204033*.

15. De Coensel, B., Botteldooren, D. and De Muer, T., 2003. 1/f noise in rural and urban soundscapes. *Acta acustica united with acustica*, *89*(2), pp.287-295.

16. Carpinteri, A., Lacidogna, G. and Accornero, F., 2018. Fluctuations of 1/f noise in damaging structures analyzed by Acoustic Emission. *Applied Sciences*, *8*(9), p.1685.

17. Friedrich, L., Colpo, A., Maggi, A., Becker, T., Lacidogna, G. and Iturrioz, I., 2021. Damage process in glass fiber reinforced polymer specimens using acoustic emission technique with low frequency acquisition. *Composite Structures*, *256*, p.113105.

18. Shannon, C.E., 2001. A mathematical theory of communication. *ACM SIGMOBILE mobile computing and communications review*, *5*(1), pp.3-55.

19. Wissner-Gross, A.D. and Freer, C.E., 2013. Causal entropic forces. *Physical review letters*, *110*(16), p.168702.

20. Mann, R.P. and Garnett, R., 2015. The entropic basis of collective behaviour. *Journal of the Royal Society Interface*, *12*(106), p.20150037.

21. Amigó, J.M., Balogh, S.G. and Hernández, S., 2018. A brief review of generalized entropies. *Entropy*, *20*(11), p.813.

22. Principe, J.C., Xu, D., Fisher, J. and Haykin, S., 2000. Information theoretic learning. *Unsupervised adaptive filtering*, *1*, pp.265-319.

23. Rényi, A., 1961. On measures of entropy and information. In *Proceedings of the Fourth Berkeley Symposium on Mathematical Statistics and Probability, Volume 1: Contributions to the Theory of Statistics*. The Regents of the University of California.

24. Tanvir, F., Sattar, T., Mba, D. and Edwards, G., 2020. Identification of fatigue damage evaluation using entropy of acoustic emission waveform. *SN Applied Sciences*, *2*(1), pp.1-15.

25. Cornforth, D.J., Tarvainen, M.P. and Jelinek, H.F., 2014. How to calculate Renyi entropy from heart rate variability, and why it matters for detecting cardiac autonomic neuropathy. *Frontiers in bioengineering and biotechnology*, *2*, p.34.

26. Coles, P.J., Berta, M., Tomamichel, M. and Wehner, S., 2017. Entropic uncertainty relations and their applications. *Reviews of Modern Physics*, *89*(1), p.015002.

27. Hartley, R.V., 1928. Transmission of information 1. *Bell System technical journal*, *7*(3), pp.535-563.

28. Shannon, C.E., 1948. A mathematical theory of communication. *The Bell system technical journal*, *27*(3), pp.379-423.

29. Csiszár, I., 1995. Generalized cutoff rates and Rényi's information measures. *IEEE Transactions on information theory*, *41*(1), pp.26-34.

30. Bennett, C.H., Brassard, G., Crépeau, C. and Maurer, U.M., 1995. Generalized privacy amplification. *IEEE Transactions on Information Theory*, *41*(6), pp.1915-1923.

31. Zhang, X., Feng, N., Wang, Y. and Shen, Y., 2015. Acoustic emission detection of rail defect based on wavelet transform and Shannon entropy. *Journal of Sound and Vibration*, *339*, pp.419-432.

32. Kankar, P.K., Sharma, S.C. and Harsha, S.P., 2011. Fault diagnosis of ball bearings using continuous wavelet transform. *Applied Soft Computing*, *11*(2), pp.2300-2312.

33. Mallat, S.G., 1989. A theory for multiresolution signal decomposition: the wavelet representation. *IEEE transactions on pattern analysis and machine intelligence*, *11*(7), pp.674-693.

34. dwt: Single-level 1-D discrete wavelet transform. https://uk.mathworks.com/help/wavelet/ref/dwt.html#References (accessed on 01/02/2021)

35. Wickerhauser, M.V., 1996. *Adapted wavelet analysis: from theory to software*. CRC Press.

36. Saeedifar, M., Najafabadi, M.A., Zarouchas, D., Toudeshky, H.H. and Jalalvand, M., 2018. Barely visible impact damage assessment in laminated composites using acoustic emission. *Composites Part B: Engineering*, *152*, pp.180-192.

37. Habibi, M. and Laperrière, L., 2020. Digital image correlation and acoustic emission for damage analysis during tensile loading of open-hole flax laminates. *Engineering Fracture Mechanics*, *228*, p.106921.

38. Mohammadi, R., Najafabadi, M.A., Saghafi, H., Saeedifar, M. and Zarouchas, D., 2021. The effect of mode II fatigue crack growth rate on the fractographic features of CFRP composite laminates: An acoustic emission and scanning electron microscopy analysis. *Engineering Fracture Mechanics*, *241*, p.107408.

39. Ameur, M.B., El Mahi, A., Rebiere, J.L., Gimenez, I., Beyaoui, M., Abdennadher, M. and Haddar, M., 2019. Investigation and identification of damage mechanisms of unidirectional carbon/flax hybrid composites using acoustic emission. *Engineering Fracture Mechanics*, *216*, p.106511.

40. Mouzakis, D.E. and Dimogianopoulos, D.G., 2019. Acoustic emission detection of damage induced by simulated environmental conditioning in carbon fiber reinforced composites. *Engineering Fracture Mechanics*, *210*, pp.422-428.

41. Ni, Q.Q. and Jinen, E., 1997. Fracture behavior and acoustic emission in bending tests on single-fiber composites. *Engineering Fracture Mechanics*, *56*(6), pp.779-796.

42. Pappas, Y.Z. and Kostopoulos, V., 2001. Toughness characterization and acoustic emission monitoring of a 2-D carbon/carbon composite. *Engineering fracture mechanics*, *68*(14), pp.1557-1573.

43. Barile, C., 2019. Innovative mechanical characterization of CFRP by using acoustic emission technique. *Engineering Fracture Mechanics*, *210*, pp.414-421.

44. ASTM D5528-13, Standard Test Method for Mode I Interlaminar Fracture Toughness of Unidirectional Fiber-Reinforced Polymer Matrix Composites, ASTM International, West Conshohocken, PA, 2013, www.astm.org

45. Barile, C., Casavola, C., Moramarco, V., Pappalettere, C. and Vimalathithan, P.K., 2020. Bonding characteristics of single-and joggled-lap CFRP specimens: Mechanical and acoustic investigations. *Applied Sciences*, *10*(5), p.1782.

46. Barile, C., Casavola, C., Pappalettera, G. and Paramsamy Kannan, V., 2020. Damage assessment of carbon fibre reinforced plastic using acoustic emission technique: experimental and numerical approach. *Structural Health Monitoring*, p.1475921720946438.

47. Barile, C., Casavola, C., Pappalettera, G. and Vimalathithan, P.K., 2020. Acoustic emission descriptors for the mechanical behavior of selective laser melted samples: An innovative approach. *Mechanics of Materials*, *148*, p.103448.

Figure 1

Click here to access/download;Figure;Figure 1.jpg

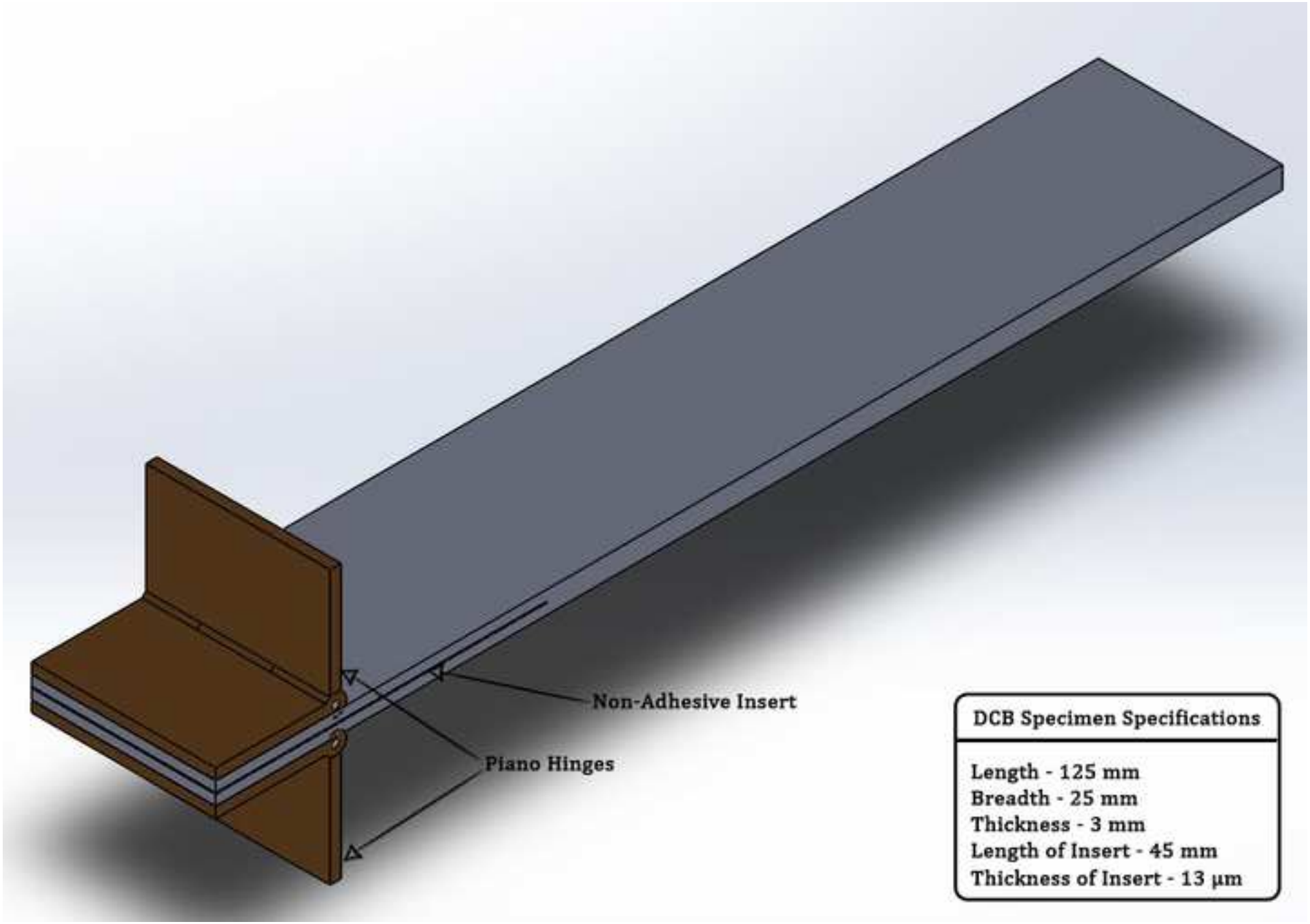

Figure 2

Click here to access/download;Figure;Figure 2.jpg

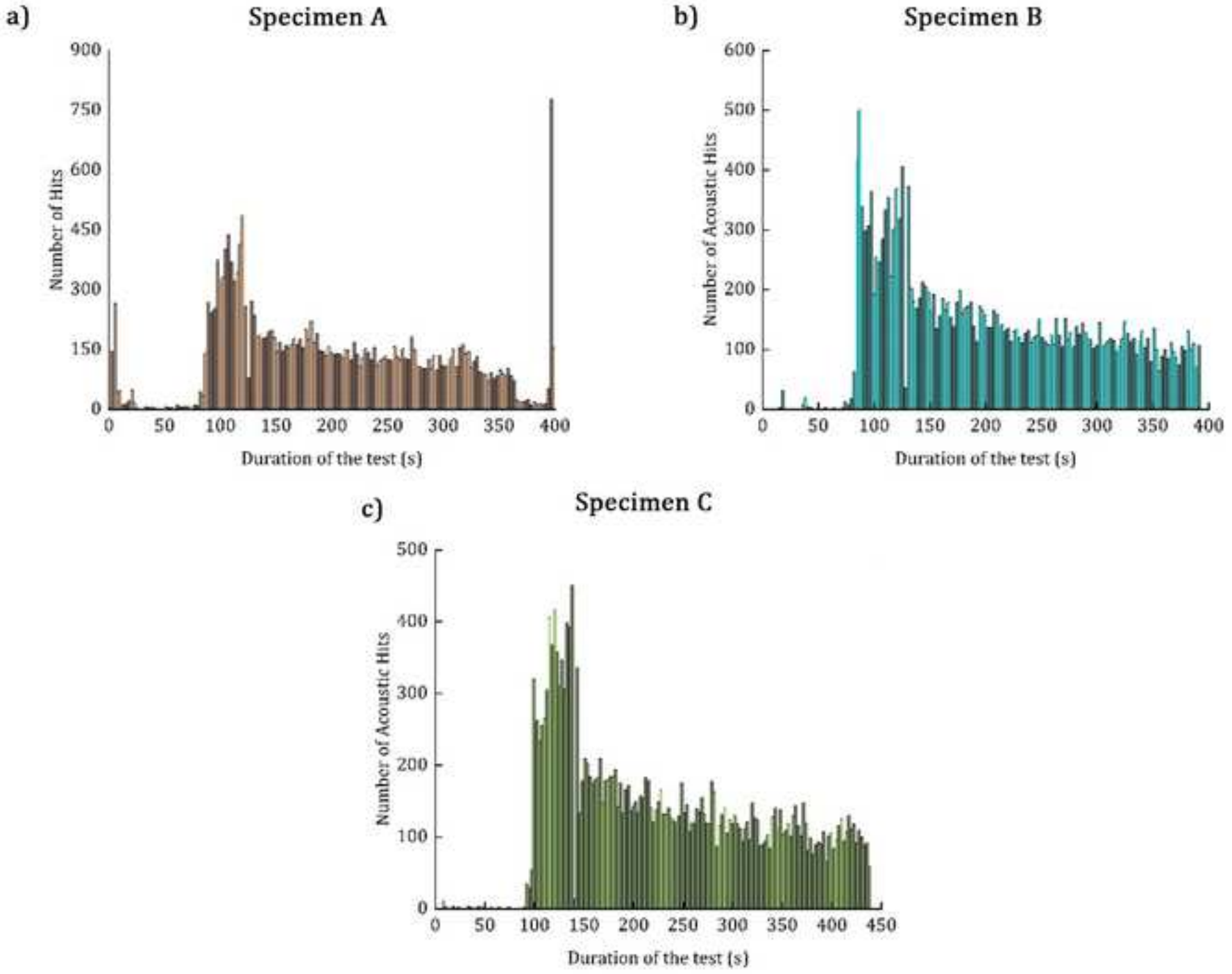

Figure 3

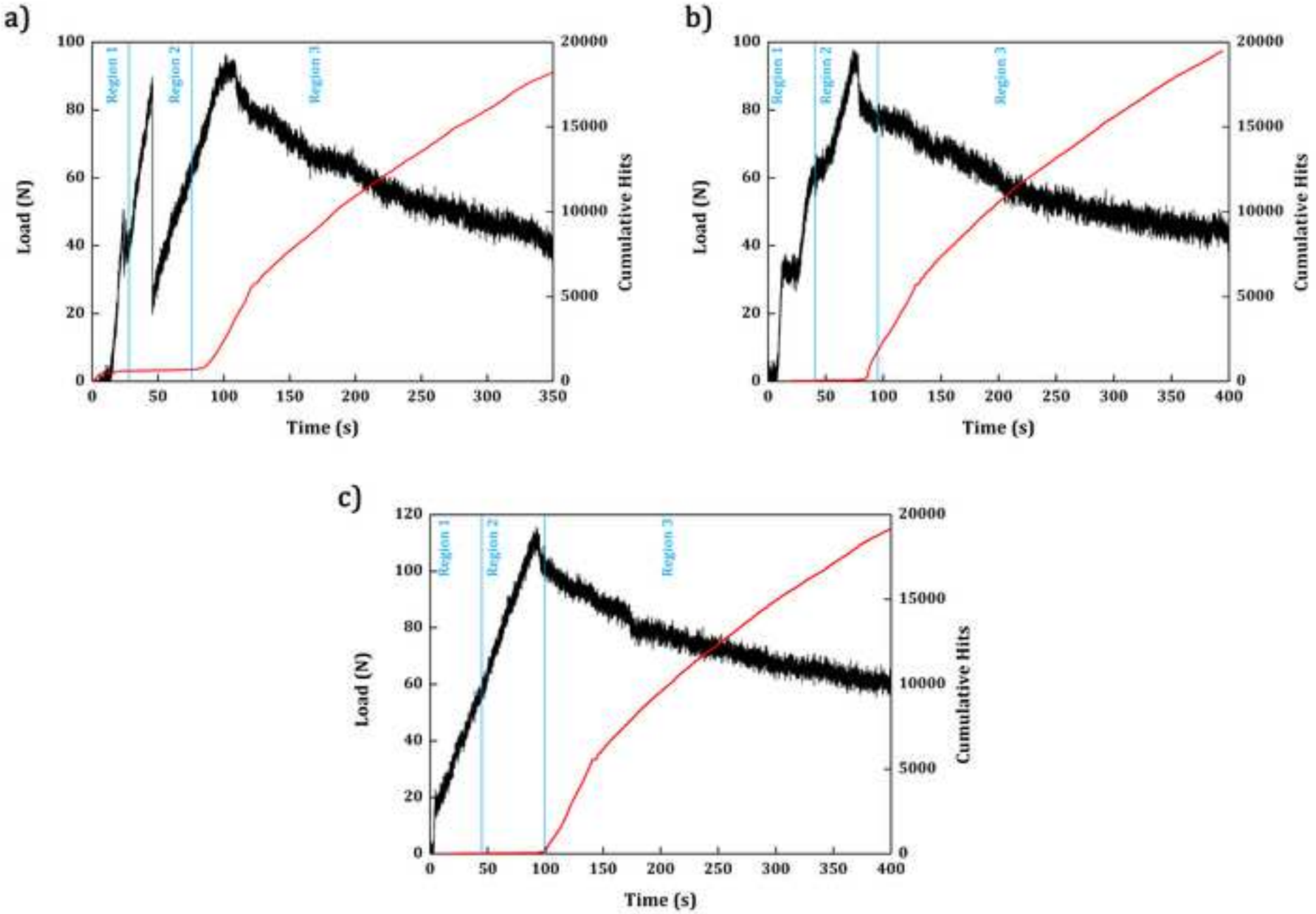

Figure 4

Click here to access/download;Figure;Figure 4.jpg

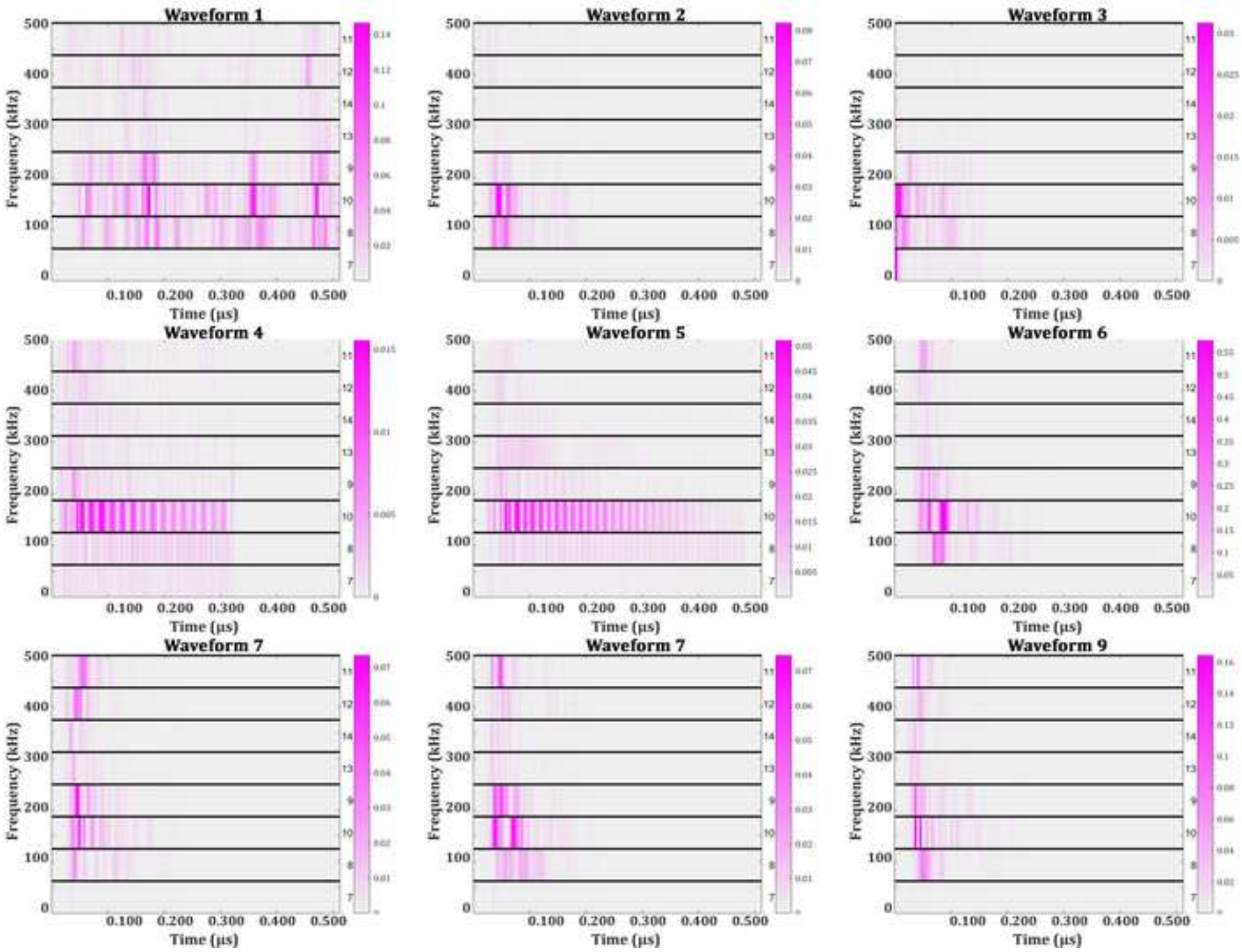

Figure 5

Click here to access/download;Figure;Figure 5.jpg

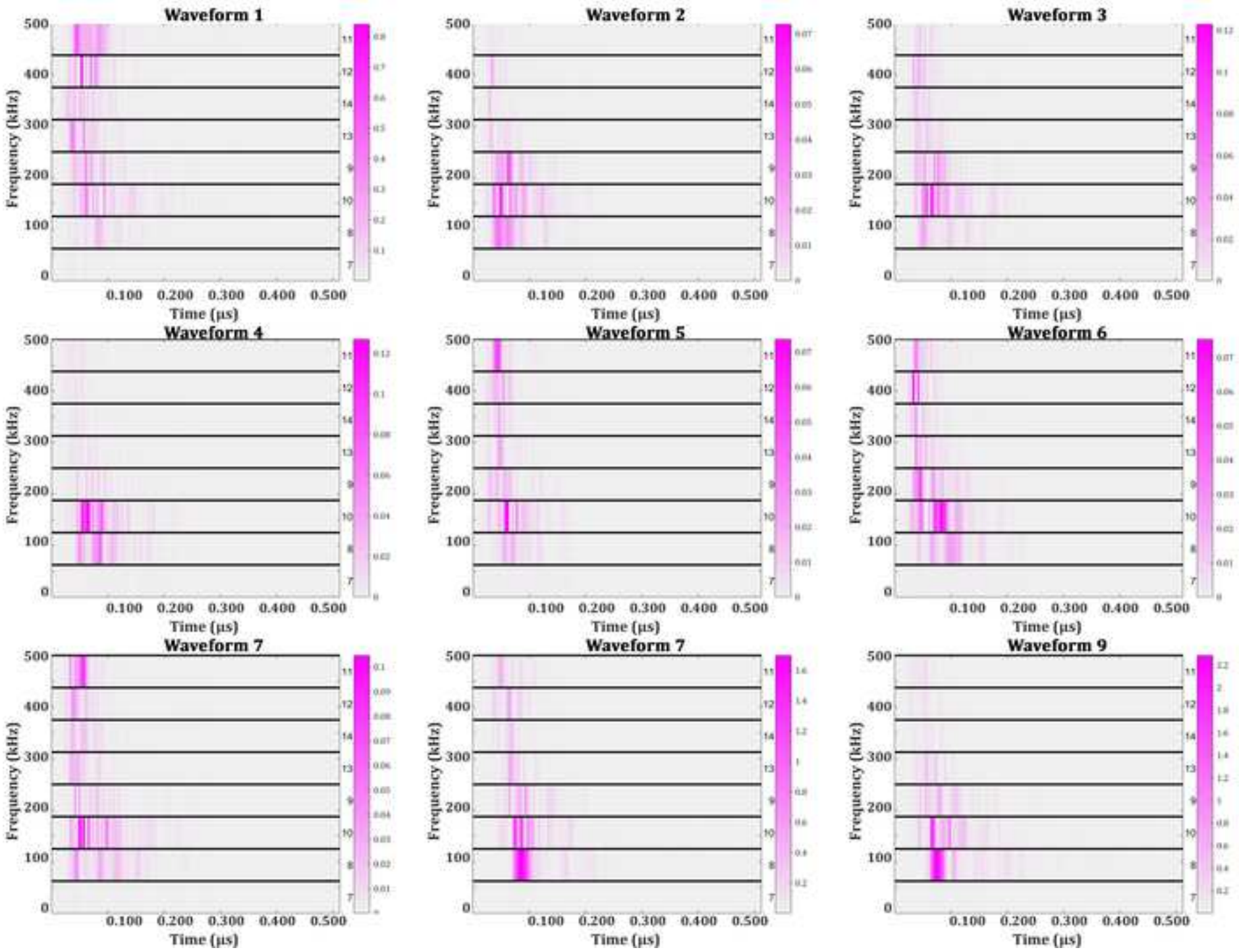

Figure 6

Click here to access/download;Figure;Figure 6.jpg

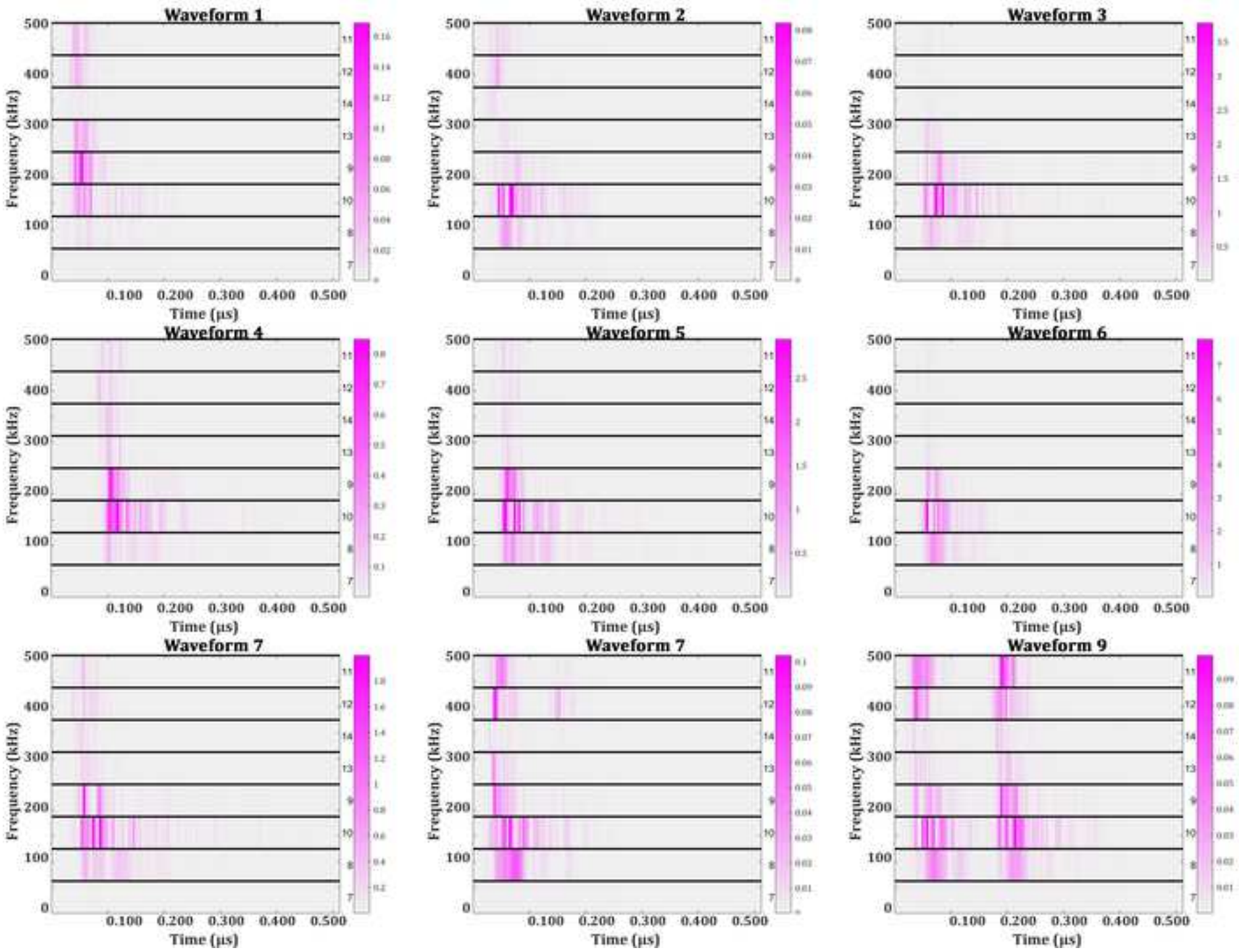

Figure 7

Click here to access/download;Figure;Figure 7.jpg

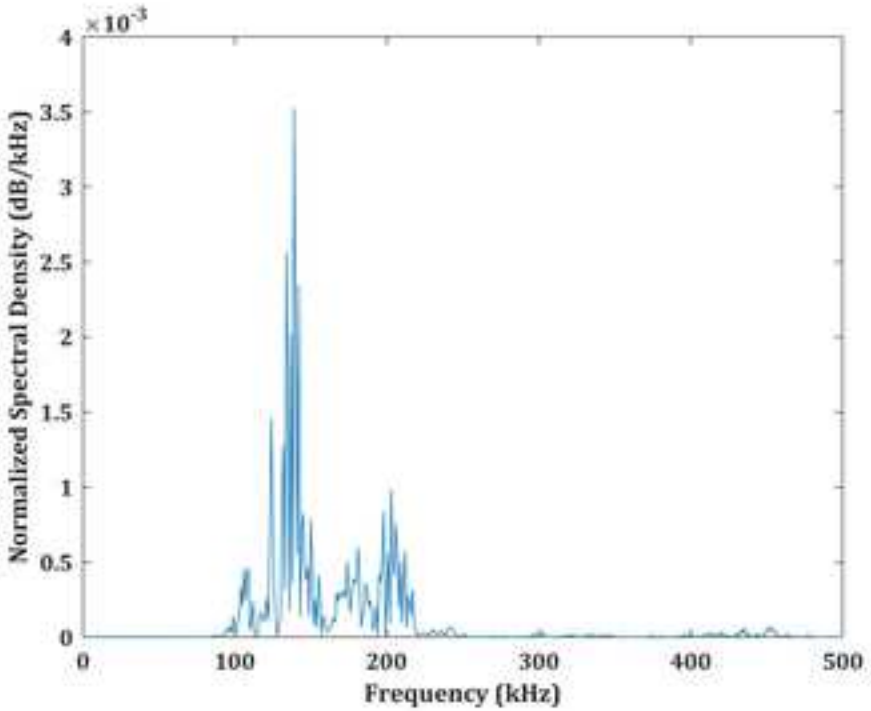

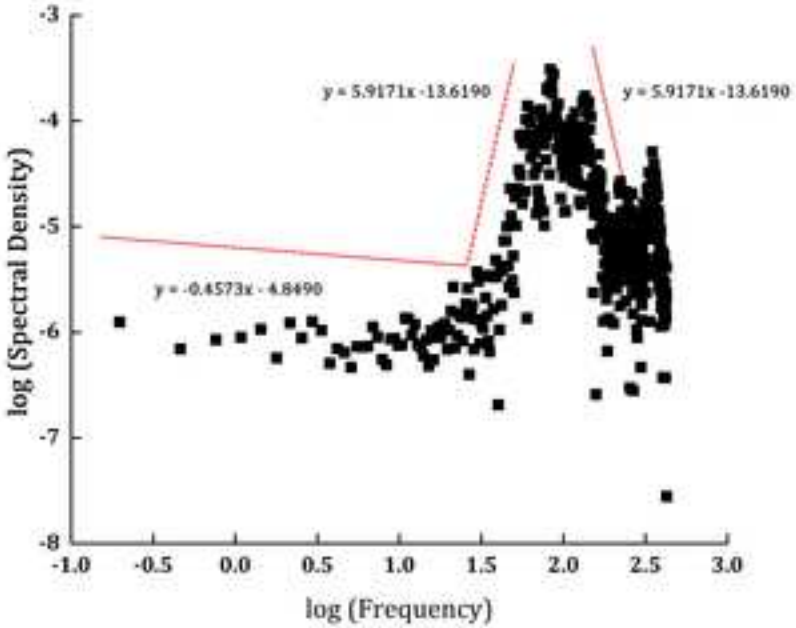

Figure 8

Click here to access/download;Figure;Figure 8.jpg

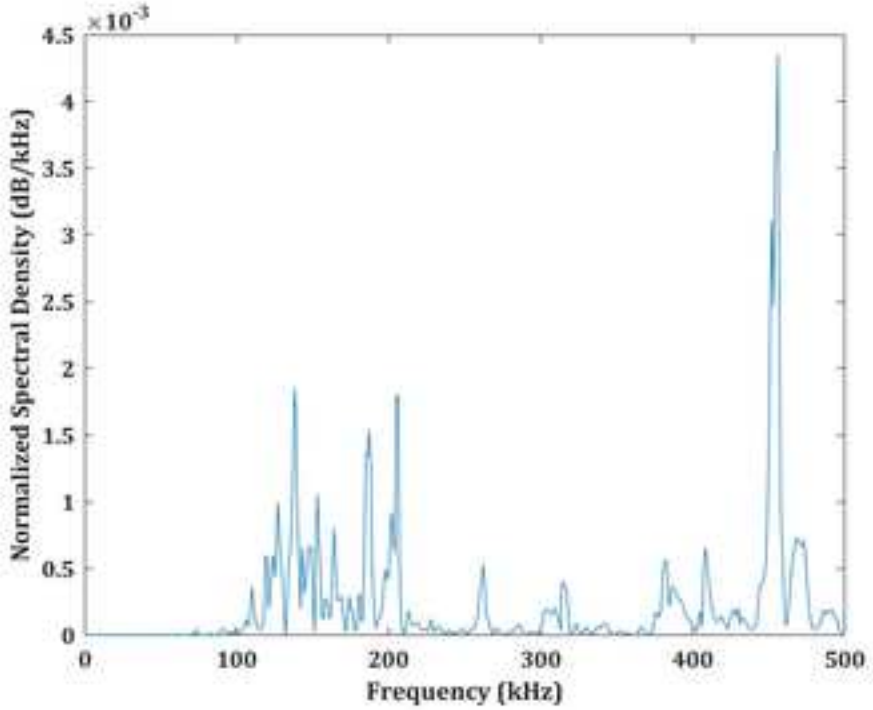

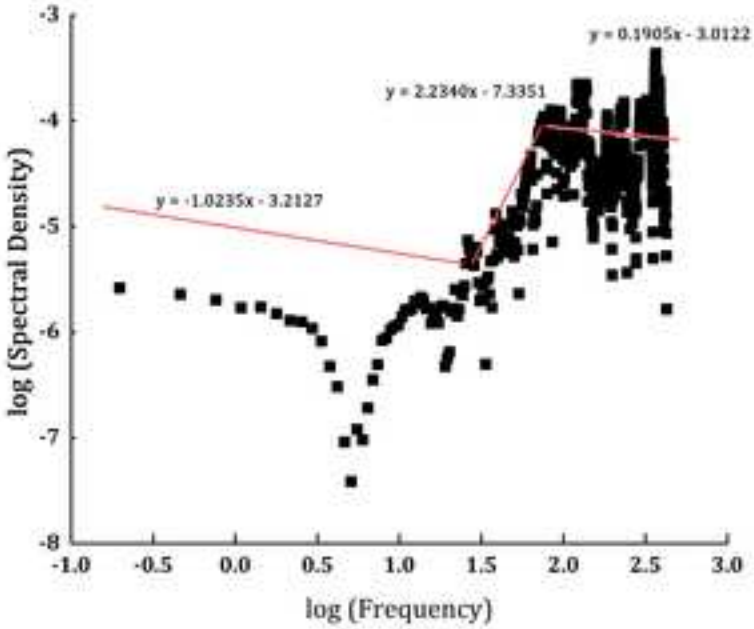

Figure 9

Click here to access/download;Figure;Figure 9.jpg

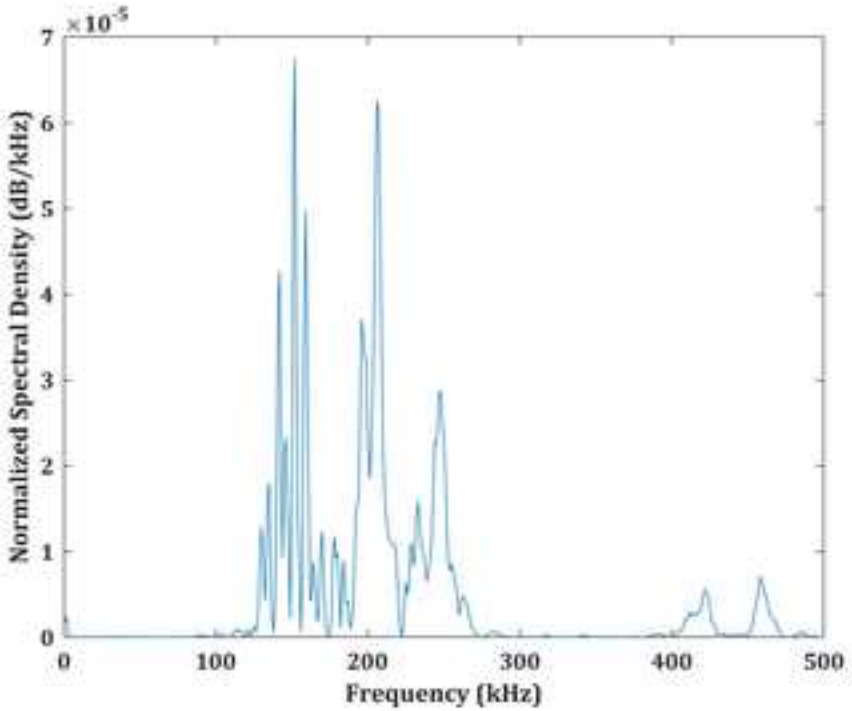

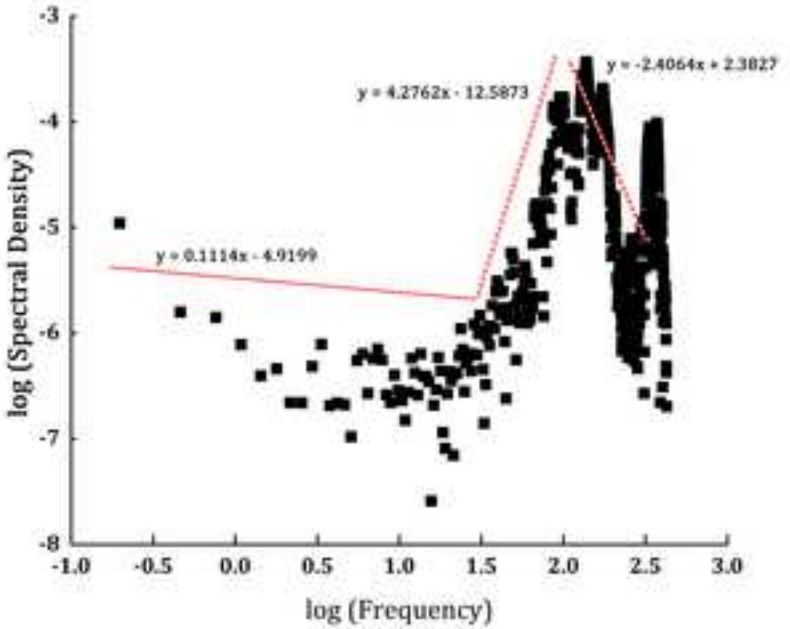

Table 1. Duration of the DCB test and the total number of Acoustic Hits recorded for all specimens

Specimen Name	**Duration of the test** *(s)*	**Number of Acoustic Hits recorded**
A	404.48	19863
B	391.68	19491
C	437.76	20797

Table 2. Wavelet Families and Wavelet selected for the analysis

S. No.	Wavelet	Wavelet Family	S. No.	Wavelet	Wavelet Family
1.	haar	Haar	13.	sym2	
2.	db1		14.	sym3	
3.	db2		15.	sym4	
4.	db3		16.	sym5	Symlet
5.	db4		17.	sym6	
6.	db5	Daubechies	18.	sym7	
7.	db6		19.	sym8	
8.	db7		20.	coif1	
9.	db8		21.	coif2	
10.	db9		22.	coif3	Coiflet
11.	db10		23.	coif4	
12.	dmey	Dmeyers	24.	coif5	

Table 3. Average quadratic Renyi's Entropy, Average Wavelet Energy, η Value and Rank based on η Value for specimens A, B and C

Wavelet	Average Entropy			Average Energy			η Value			Rank		
	A	B	C	A	B	C	A	B	C	A	B	C
haar	1.5701	1.6915	1.6237	0.0031	0.0041	0.0042	0.002	0.00242	0.0026	23	23	23
db1	1.5701	1.6915	1.6237	0.0031	0.0041	0.0042	0.002	0.00242	0.0026	23	23	23
db2	1.4407	1.5809	1.4977	0.0034	0.0043	0.0045	0.00237	0.00272	0.00305	19	19	20
db3	1.4844	1.6257	1.5432	0.0035	0.0045	0.0047	0.00239	0.00273	0.00308	17	17	17
db4	1.5699	1.6915	1.6230	0.0036	0.0045	0.0048	0.0023	0.00268	0.003	22	22	22
db5	1.5251	1.6587	1.5809	0.0037	0.0046	0.0049	0.00241	0.00277	0.00314	15	14	14
db6	1.5172	1.6549	1.5802	0.0037	0.0046	0.0050	0.00245	0.0028	0.00319	9	7	7
db7	1.5590	1.6836	1.6164	0.0037	0.0047	0.0050	0.0024	0.00275	0.00313	16	16	15
db8	1.5570	1.6842	1.6124	0.0038	0.0047	0.0050	0.00242	0.00276	0.00315	13	15	13
db9	1.5356	1.6700	1.5979	0.0038	0.0047	0.0051	0.00247	0.00279	0.00319	4	10	6
db10	1.5479	1.6766	1.6080	0.0038	0.0047	0.0051	0.00246	0.0028	0.00317	7	9	10
sym2	1.4407	1.5809	1.4977	0.0034	0.0043	0.0045	0.00237	0.00272	0.00305	19	19	20
sym3	1.4844	1.6257	1.5432	0.0035	0.0045	0.0047	0.00239	0.00273	0.00308	17	17	17
sym4	1.4945	1.6332	1.5552	0.0036	0.0045	0.0048	0.00243	0.00277	0.00316	12	13	11
sym5	1.5659	1.6894	1.6217	0.0037	0.0046	0.0049	0.00235	0.0027	0.00306	21	21	19
sym6	1.5198	1.6547	1.5821	0.0037	0.0046	0.0050	0.00246	0.0028	0.00318	8	8	9
sym7	1.5338	1.6674	1.5950	0.0038	0.0047	0.0050	0.00245	0.00278	0.00316	11	12	12
sym8	1.5325	1.6649	1.5954	0.0038	0.0047	0.0050	0.00247	0.0028	0.0032	5	5	5
coif1	1.4179	1.5615	1.4764	0.0034	0.0044	0.0045	0.00242	0.00279	0.00313	14	11	16
coif2	1.4848	1.6263	1.5468	0.0036	0.0046	0.0049	0.00245	0.0028	0.00319	10	6	8
coif3	1.5141	1.6517	1.5780	0.0037	0.0047	0.0050	0.00247	0.00281	0.0032	6	4	4
coif4	1.5288	1.6635	1.5933	0.0038	0.0047	0.0051	0.00248	0.00282	0.0032	3	3	3
coif5	1.5373	1.6698	1.6012	0.0038	0.0047	0.0051	0.00248	0.00283	0.00321	2	2	2
dmey	1.5542	1.6833	1.6154	0.0039	0.0048	0.0052	0.00251	0.00285	0.00323	1	1	1

Table 4. WPT components for the selected waveforms from Specimen A calculated using selected wavelets coif4, coif5 and dmey

Components	1	2	3	4	5	6	7	8
	Frequency Range (kHz)							
	0-62.5	**62.5-125**	**125-187.5**	**187.5-250**	**250-312.5**	**312.5-375**	**375-437.5**	**437.5-500**
	coif4							
Waveform 1	0.0011	0.8126	1.3033	0.3268	0.0808	0.0242	0.0699	0.0328
Waveform 2	0.0003	0.1198	0.1384	0.0063	0.0012	0.0011	0.0007	0.0012
Waveform 3	0.0137	0.0100	0.0112	0.0011	0.0002	0.0001	0.0000	0.0000
Waveform 4	0.0005	0.0020	0.0239	0.0031	0.0004	0.0008	0.0003	0.0008
Waveform 5	0.0009	0.0162	0.2638	0.0176	0.0074	0.0070	0.0014	0.0010
Waveform 6	0.0121	4.9908	11.1268	0.9565	0.3307	0.1761	0.4993	0.6104
Waveform 7	0.0006	0.0321	0.0615	0.0709	0.0129	0.0131	0.0635	0.0203
Waveform 8	0.0004	0.0425	0.1969	0.0838	0.0076	0.0053	0.0145	0.0411
Waveform 9	0.0004	0.2295	0.4102	0.0979	0.0720	0.0142	0.0523	0.0687
	coif5							
Waveform 1	0.0007	0.7968	1.3085	0.3498	0.0656	0.0286	0.0622	0.0369
Waveform 2	0.0003	0.1138	0.1447	0.0066	0.0008	0.0007	0.0010	0.0010
Waveform 3	0.0107	0.0111	0.0088	0.0011	0.0002	0.0000	0.0001	0.0000
Waveform 4	0.0005	0.0019	0.0248	0.0026	0.0004	0.0006	0.0004	0.0007
Waveform 5	0.0008	0.0151	0.2716	0.0140	0.0070	0.0046	0.0013	0.0009
Waveform 6	0.0119	4.7893	11.3300	1.0321	0.3498	0.1151	0.1620	0.9123
Waveform 7	0.0005	0.0303	0.0647	0.0729	0.0163	0.0080	0.0506	0.0318
Waveform 8	0.0004	0.0415	0.1978	0.0863	0.0085	0.0033	0.0093	0.0450
Waveform 9	0.0005	0.2225	0.4184	0.1075	0.0433	0.0338	0.0320	0.0871
	dmey							
Waveform 1	0.0008	0.7050	1.3288	0.4550	0.0323	0.0240	0.0685	0.0324
Waveform 2	0.0003	0.0787	0.1797	0.0078	0.0003	0.0003	0.0009	0.0010
Waveform 3	0.0085	0.0099	0.0246	0.0011	0.0001	0.0000	0.0000	0.0000
Waveform 4	0.0004	0.0018	0.0268	0.0011	0.0003	0.0003	0.0003	0.0008
Waveform 5	0.0007	0.0131	0.2844	0.0074	0.0064	0.0010	0.0015	0.0008
Waveform 6	0.0090	3.8303	12.0554	1.4629	0.1714	0.0867	0.1980	0.8891
Waveform 7	0.0005	0.0205	0.0813	0.0774	0.0061	0.0061	0.0425	0.0405
Waveform 8	0.0004	0.0368	0.1973	0.0963	0.0028	0.0037	0.0079	0.0469
Waveform 9	0.0005	0.1788	0.4524	0.1508	0.0184	0.0232	0.0356	0.0856

Table 5. WPT components for the selected waveforms from Specimen B calculated using selected wavelets coif4, coif5 and dmey

Components	1	2	3	4	5	6	7	8
	Frequency (kHz)							
	0-62.5	62.5-125	125-187.5	187.5-250	250-312.5	312.5-375	375-437.5	437.5-500
	coif4							
Waveform 1	0.0100	1.2638	4.5890	2.6518	3.7288	4.0272	6.0455	11.6300
Waveform 2	0.0003	0.0767	0.0955	0.0517	0.0085	0.0025	0.0052	0.0014
Waveform 3	0.0003	0.0603	0.3122	0.0651	0.0316	0.0056	0.0385	0.0077
Waveform 4	0.0010	0.2206	0.4965	0.0168	0.0052	0.0034	0.0040	0.0030
Waveform 5	0.0003	0.0255	0.0957	0.0119	0.0116	0.0089	0.0360	0.0395
Waveform 6	0.0003	0.0617	0.1926	0.0613	0.0240	0.0087	0.0604	0.0268
Waveform 7	0.0007	0.0637	0.2881	0.0236	0.0333	0.0231	0.0621	0.1462
Waveform 8	0.0412	112.2750	42.2921	9.2358	6.8401	2.3913	4.6629	5.8199
Waveform 9	0.0813	187.7207	62.9372	12.0722	6.1573	2.1790	0.9247	1.2256
	coif5							
Waveform 1	0.0249	1.2082	4.6087	2.7739	4.2295	1.5373	10.8631	8.7005
Waveform 2	0.0003	0.0747	0.0973	0.0537	0.0069	0.0043	0.0045	0.0003
Waveform 3	0.0003	0.0572	0.3143	0.0694	0.0275	0.0148	0.0276	0.0101
Waveform 4	0.0009	0.2158	0.5034	0.0163	0.0052	0.0029	0.0032	0.0029
Waveform 5	0.0003	0.0238	0.0972	0.0124	0.0101	0.0065	0.0212	0.0579
Waveform 6	0.0004	0.0586	0.1961	0.0628	0.0186	0.0245	0.0524	0.0225
Waveform 7	0.0008	0.0637	0.2889	0.0242	0.0313	0.0248	0.0334	0.1738
Waveform 8	0.0253	110.6963	44.1473	9.4265	6.5663	2.4050	5.7781	4.5133
Waveform 9	0.1098	185.7518	65.2298	12.3971	6.2414	1.2615	0.8674	1.4391
	dmey							
Waveform 1	0.0181	1.0502	4.8722	3.1186	3.9154	1.4586	9.4853	10.0276
Waveform 2	0.0003	0.0669	0.1030	0.0597	0.0039	0.0028	0.0049	0.0005
Waveform 3	0.0003	0.0439	0.3154	0.0926	0.0164	0.0117	0.0311	0.0099
Waveform 4	0.0009	0.1878	0.5350	0.0150	0.0036	0.0021	0.0033	0.0030
Waveform 5	0.0003	0.0154	0.1042	0.0142	0.0097	0.0067	0.0170	0.0619
Waveform 6	0.0004	0.0417	0.2173	0.0654	0.0174	0.0122	0.0603	0.0213
Waveform 7	0.0007	0.0667	0.2865	0.0286	0.0279	0.0225	0.0415	0.1663
Waveform 8	0.0221	102.9391	51.9988	10.7906	5.5359	2.0438	5.6804	4.5484
Waveform 9	0.0836	169.9488	81.1800	13.5344	5.7209	0.5893	0.8890	1.3532

Table 6. WPT components for the selected waveforms from Specimen C calculated using selected wavelets coif4, coif5 and dmey

Components	1	2	3	4	5	6	7	8
	Frequency (kHz)							
	0-62.5	62.5-125	125-187.5	187.5-250	250-312.5	312.5-375	375-437.5	437.5-500
	coif4							
Waveform 1	0.0004	0.0250	0.2436	0.4084	0.1619	0.0131	0.0496	0.0445
Waveform 2	0.0003	0.0569	0.1695	0.0093	0.0017	0.0029	0.0098	0.0048
Waveform 3	0.0475	55.5520	352.2950	53.4341	12.4369	3.7574	0.3939	0.4109
Waveform 4	0.0100	2.2053	22.0602	10.6188	1.1518	2.0988	0.4384	0.5529
Waveform 5	0.1005	86.1163	232.7857	150.8409	5.3079	3.7312	2.3556	2.8181
Waveform 6	0.1079	495.3054	827.9057	185.6956	22.3903	7.3477	1.5056	2.6723
Waveform 7	0.0330	23.2480	108.0183	55.5821	2.0926	2.6129	1.8316	3.3009
Waveform 8	0.0004	0.2730	0.2200	0.1022	0.0297	0.0212	0.1488	0.0592
Waveform 9	0.0009	0.2068	0.4726	0.1782	0.0334	0.0290	0.2579	0.1964
	coif5							
Waveform 1	0.0005	0.0214	0.2382	0.4310	0.1539	0.0030	0.0526	0.0460
Waveform 2	0.0003	0.0529	0.1749	0.0088	0.0015	0.0016	0.0119	0.0031
Waveform 3	0.0486	50.5132	360.8346	52.6634	11.2019	2.4818	0.2039	0.3818
Waveform 4	0.0063	2.0418	22.7027	10.6738	1.4802	1.2969	0.4771	0.4579
Waveform 5	0.1042	81.7200	243.7455	146.8233	3.1458	3.4278	2.2421	2.8489
Waveform 6	0.0594	477.3133	853.4198	185.4775	17.0469	5.3147	1.6842	2.6150
Waveform 7	0.0140	21.6454	111.6079	54.4280	1.9643	1.7938	3.0485	2.2176
Waveform 8	0.0004	0.2685	0.2280	0.1014	0.0326	0.0052	0.1582	0.0603
Waveform 9	0.0007	0.1999	0.4844	0.1797	0.0364	0.0111	0.1752	0.2878
	dmey							
Waveform 1	0.0004	0.0095	0.1976	0.5266	0.1121	0.0013	0.0511	0.0480
Waveform 2	0.0003	0.0319	0.1993	0.0064	0.0012	0.0011	0.0108	0.0040
Waveform 3	0.0348	30.3107	391.5161	49.1360	6.5337	0.2048	0.1742	0.4185
Waveform 4	0.0035	1.3234	24.1031	11.3214	0.7512	0.6673	0.5271	0.4390
Waveform 5	0.0523	62.9700	292.8911	118.8699	2.3699	1.7043	2.0175	3.1828
Waveform 6	0.0615	389.1842	977.9529	164.6860	5.9834	0.9105	1.5637	2.5961
Waveform 7	0.0119	14.1017	124.8928	48.2363	2.5962	1.5289	2.9626	2.3889
Waveform 8	0.0004	0.2382	0.2671	0.0955	0.0310	0.0022	0.1399	0.0803
Waveform 9	0.0007	0.1642	0.5332	0.1802	0.0222	0.0096	0.1638	0.3013

Table 7. Spectral Energy Percentage of the Waveforms recorded from Specimen A

Components	1	2	3	4	5	6	7	8
	Frequency (kHz)/ % of Spectral Energy							
	0-62.5	62.5-125	125-187.5	187.5-250	250-312.5	312.5-375	375-437.5	437.5-500
Region 1								
Waveform 1	0.0286	26.6387	50.2044	17.1903	1.2211	0.9068	2.5865	1.2237
Waveform 2	0.1093	29.2578	66.7988	2.8966	0.1173	0.0954	0.3525	0.3723
Waveform 3	19.2562	22.3977	55.3756	2.4838	0.2275	0.0892	0.0947	0.0754
Region 2								
Waveform 4	1.3806	5.5336	84.3540	3.4569	0.9904	0.8755	0.9717	2.4373
Waveform 5	0.2279	4.1530	90.1919	2.3611	2.0320	0.3141	0.4723	0.2478
Waveform 6	0.0481	20.4797	64.4579	7.8216	0.9164	0.4635	1.0588	4.7540
Region 3								
Waveform 7	0.1870	7.4568	29.5793	28.1473	2.2242	2.2307	15.4372	14.7375
Waveform 8	0.0920	9.3943	50.3151	24.5695	0.7224	0.9394	2.0164	11.9508
Waveform 9	0.0511	18.9115	47.8564	15.9574	1.9465	2.4507	3.7713	9.0552

Table 8. Spectral Energy Percentage of the Waveforms recorded from Specimen B

Components	1	2	3	4	5	6	7	8
	Frequency (kHz)/ % of Spectral Energy							
	0-62.5	62.5-125	125-187.5	187.5-250	250-312.5	312.5-375	375-437.5	437.5-500
Region 1								
Waveform 1	0.0534	3.0937	14.3527	9.1870	11.5343	4.2969	27.9423	29.5398
Waveform 2	0.1052	27.6671	42.5712	24.6765	1.6174	1.1644	2.0119	0.1862
Waveform 3	0.0503	8.4261	60.5168	17.7594	3.1385	2.2472	5.9714	1.8901
Region 2								
Waveform 4	0.1239	25.0138	71.2757	1.9960	0.4732	0.2771	0.4443	0.3961
Waveform 5	0.1220	6.6935	45.4366	6.1914	4.2376	2.9234	7.4025	26.9929
Waveform 6	0.0879	9.5629	49.8374	14.9925	3.9906	2.8048	13.8277	4.8962
Region 3								
Waveform 7	0.1123	10.4151	44.7058	4.4696	4.3571	3.5135	6.4793	25.9473
Waveform 8	0.0121	56.0795	28.3281	5.8785	3.0158	1.1134	3.0946	2.4779
Waveform 9	0.0306	62.1842	29.7037	4.9522	2.0933	0.2156	0.3253	0.4951

Table 9. Spectral Energy Percentage of the Waveforms recorded from Specimen C

Components	1	2	3	4	5	6	7	8
	Frequency (kHz)/ % of Spectral Energy							
	0-62.5	62.5-125	125-187.5	187.5-250	250-312.5	312.5-375	375-437.5	437.5-500
Region 1								
Waveform 1	0.0439	1.0081	20.8770	55.6257	11.8393	0.1355	5.3958	5.0747
Waveform 2	0.0989	12.5215	78.1532	2.5261	0.4547	0.4290	4.2398	1.5768
Waveform 3	0.0073	6.3368	81.8508	10.2724	1.3660	0.0428	0.0364	0.0875
Region 2								
Waveform 4	0.0091	3.3816	61.5881	28.9283	1.9195	1.7050	1.3467	1.1216
Waveform 5	0.0108	13.0088	60.5075	24.5570	0.4896	0.3521	0.4168	0.6575
Waveform 6	0.0040	25.2236	63.3825	10.6735	0.3878	0.0590	0.1013	0.1683
Region 3								
Waveform 7	0.0061	7.1684	63.4878	24.5204	1.3197	0.7772	1.5060	1.2144
Waveform 8	0.0449	27.8760	31.2586	11.1723	3.6319	0.2533	16.3685	9.3945
Waveform 9	0.0514	11.9430	38.7748	13.1012	1.6150	0.6964	11.9126	21.9055

Table 10. Shifting in the Spectral Density of the Waveforms recorded from testing Specimen A

Waveform	Stage I		Stage II		Stage III		Apparent Damage Mode
	Slope	Intercept	Slope	Intercept	Slope	Intercept	
Region 1							
1	-0.6640	-4.4237	3.6878	-10.6125	-3.9015	5.8645	Matrix Cracking
2	-0.5968	-4.2201	4.3961	-12.3821	-5.6514	9.0136	
3	-0.4940	-3.9640	2.0150	-7.7331	-3.4640	3.9058	
Region 2							
4	-0.3496	-4.3836	1.7525	-7.9480	-4.2454	5.6306	Delamination
5	-0.0254	-4.6773	2.6653	-9.3787	-1.8230	0.3031	
6	-0.6370	-4.3267	3.7380	-10.1668	-2.6676	3.4281	Matrix Cracking
Region 3							
7	-0.4097	-4.1436	4.0405	-11.8661	0.1617	-3.7295	Crack Growth
8	-0.3930	-4.1502	3.9727	-11.4893	-0.7370	-1.9060	
9	-0.2389	-4.3428	4.7180	-12.9693	-0.8401	-1.3191	

Table 11. Shifting in the Spectral Density of the Waveforms recorded from testing Specimen B

Waveform	Stage I		Stage II		Stage III		Apparent Damage Mode
	Slope	Intercept	Slope	Intercept	Slope	Intercept	
Region 1							
1	-0.7418	-3.3487	1.9685	-6.8162	-0.5640	-3.9791	Crack Growth
2	-0.3499	-4.4746	3.7007	-11.2724	-1.8608	0.6889	Delamination
3	-0.4918	-4.3752	4.5484	-12.7920	-1.4157	-0.1247	
Region 2							
4	-0.7803	-4.0928	3.6909	-10.6266	-1.9981	0.9767	Matrix Cracking
5	-0.5026	-4.2865	6.0837	-6.0567	-1.7740	0.5130	Crack Growth
6	-0.4776	-4.2704	3.0698	9.9496	-0.2144	-3.0559	
Region 3							
7	-0.6068	-4.0984	3.2416	-9.8888	-0.1288	-3.2361	Crack Growth
8	-0.7555	-2.9042	3.3907	-9.1268	-1.1488	0.3988	Matrix Cracking
9	-0.7026	-2.8965	3.3960	-8.6428	-2.5325	3.6833	

Table 12. Shifting in the Spectral Density of the Waveforms recorded from testing Specimen C

Waveform	Stage I		Stage II		Stage III		Apparent Damage Mode
	Slope	Intercept	Slope	Intercept	Slope	Intercept	
Region 1							
1	0.1114	-4.9199	4.2762	-12.5873	-2.4064	2.3827	Not assigned
2	-0.5876	-4.2878	7.0606	-18.3390	-4.0625	5.5607	Matrix Cracking
3	-0.7489	-2.8907	5.2763	-12.7830	-3.7119	6.5239	
Region 2							
4	-0.1251	-3.7998	3.8120	-10.5922	-2.7713	4.1559	Delamination
5	-0.8573	-2.8139	4.5481	-11.1480	-6.6142	13.1717	
6	-0.9483	-2.6536	4.5334	-11.2057	-3.8895	7.0770	
Region 3							
7	-0.7559	-3.0025	4.4631	-11.4727	-2.2553	3.2176	Delamination
8	-0.4279	-4.3031	7.1647	-18.0282	-0.6344	-1.9603	Crack Growth
9	-0.2417	-4.4425	3.9734	-11.5034	-0.4394	-2.3279	